

# To what extent is the description of streets important in estimating local air-quality? A case study over Paris.

Alexis Squarcioni<sup>1,2</sup>, Yelva Roustan<sup>1,\*</sup>, Myrto Valari<sup>2,\*</sup>, Youngseob Kim<sup>1</sup>, Karine Sartelet<sup>1</sup>, Lya Lugon<sup>1</sup>, Fabrice Dugay<sup>3</sup>, and Robin Voitot<sup>3</sup>

<sup>1</sup>CEREA, École des Ponts, EDF R&D, Marne-la-Vallée, France

<sup>2</sup>Laboratoire de Météorologie Dynamique, Sorbonne Université, Ecole Polytechnique, IPSL, École Normale Supérieure, CNRS, Paris, France

<sup>3</sup>AIRPARIF, 75004, Paris, France

\*These authors contributed equally to this work.

**Correspondence:** Alexis Squarcioni (alexis.squarcioni@enpc.fr) and Yelva Roustan (yelva.roustan@enpc.fr)

**Abstract.** Modelling atmospheric composition at street level is challenging because pollutant concentration within street canyons depends on both local emissions and the transport of polluted air masses from remote areas. Therefore, regional-scale modelling and local applications must be combined to provide accurate simulations of the atmospheric composition at street locations. In our study, we compare two strategies: i) a subgrid-scale approach embedded in the chemistry-transport model or ii) the street-network model MUNICH. In both cases, the regional-scale chemistry-transport model CHIMERE provides the urban background concentrations, and the meteorological model WRF, coupled with CHIMERE, is used to provide meteorological fields. Simulation results for NO<sub>x</sub>, NO<sub>2</sub>, and PM<sub>2.5</sub> concentrations over the city of Paris from both modelling approaches are compared with in-situ measurements in traffic air-quality stations. At stations located in downtown areas, with low traffic emissions, the street-network model MUNICH exhibits superior performance compared to the Subgrid approach for NO<sub>x</sub> concentrations, while comparable results are obtained for NO<sub>2</sub>. However, significant discrepancies between the two methods are observed for all analyzed pollutants at stations heavily influenced by road traffic. These stations are typically located near highways, where the [bias-difference](#) between the two approaches can reach 58%. The Subgrid approach's ability to estimate accurate emissions data is limited, leading to potential underestimation or overestimation of gas and fine particle concentrations based on the emission heterogeneity it handles. The performance of MUNICH appears to be highly sensitive to the friction velocity, a parameter influenced by the anthropogenic heat flux used in the WRF model. Street dimensions do contribute to the performance disparities observed between the two approaches, yet emissions remain the predominant factor.

## 1 Introduction

Numerous research studies [assess-assessed](#) the consequences of atmospheric pollutants in terms of harmful health effects and premature deaths (WHO, 2013, 2021) as well as the impacts on ecosystems and biodiversity (Marcoa et al., 2019; WGE, 2016). A vast majority of world's cities suffer from significant atmospheric pollution problems (Sicard et al., 2023), representing a prominent threat to human health and the global environment. A significant part of the European population is exposed to

concentrations above the limit or target values (EEA, 2023). Exposure to high concentration of particulate matter are one of the most harmful agents of atmospheric pollution (Lelieveld et al., 2015).

25 Results from these investigations motivate progress in air-quality modelling, in order to estimate more precisely pollutant concentration and dispersion at decisive (i.e local) spatial scales (Lugon et al., 2022). Models are valuable to understand and support the control of the evolution of air quality inside cities.

Several approaches exist to assess air pollutant concentration at local scale in urban built environments. The scientific and practical relevance of their use depends on the objectives and issues to be addressed. As explained in Kiesewetter et al. (2013),  
30 local estimations of gas or particulate matter concentrations are obtainable from regional modelling by the implementation of downscaling coefficients to determine urban and roadside increments. Despite variations on the mathematical implementation, the general methodology of the local increments has been used (Lenschow et al., 2001) and it is based on the estimation of the impact of the city and of the local traffic, added to the regional background.

However, some research studies (Longley et al., 2014; Thunis, 2017) highlight the dependence of these local increments  
35 on crucial parameters such as wind direction, wind speed, and station location. The implicit empirical adjustment inherent in this type of approach, based on statistical processing of observation data, makes them difficult to ~~transpose~~ transfer from one city to another. Alternative statistical methods introducing more explicitly site specific geographical information exist and can be efficient in terms of computation time or quantity of necessary data. For instance Land-Use Regression (LUR) models (Azmi et al., 2023; Dons et al., 2013) based on regression methods to solve the spatial variability of concentrations through  
40 a set of spatialized information (traffic, population density, ...), are often used in dense urban areas. However, as reported in Hatzopoulou et al. (2017), LUR models are robust only in regions where dense measured data are available. The number of necessary data for optimum results could change from one city to another, depending on the urban density.

In the range of methods based on ~~a globally-deterministic~~ first principles approach (i.e. resolution of conservation equations) the Computational Fluid Dynamics models (CFD) provide very fine description of air pollution concentrations at street-scale.  
45 This modelling technique handles extremely intricate wall shapes and other boundary conditions through the use of flexible fine-scale grids. Additionally, CFD models incorporate advanced approaches to take into account turbulence, making it well-suited for applications involving small-scale dispersion of pollutants. This type of model is widely used to analyse specific urban configuration on a neighbourhood scale (Sabatino et al., 2013; Zhang et al., 2020; Pantusheva et al., 2022; Lin et al., 2023), but the computing times ~~virtually requested~~ required to simulate a large urban area over periods of time of the order  
50 of a year are currently unattainable. With this type of temporal and spatial constraint, compatible with regulatory objectives (for example, compliance with a threshold for an annual average concentration) or a health impact study, methods with lower computational burdens are currently mandatory. Deterministic models, relying on simplified representations of street topology and atmospheric flow in streets have been developed for years. In this category we can mention the Operational Street Pollution Model (OSPM, Berkowicz, 2000) and its evolution in Atmospheric Dispersion Modelling System (ADMS-urban, Stocker et al.,  
55 2012). These models combine a Gaussian plume to estimate the direct contributions of traffic emissions and a box model to calculate the background concentration in the recirculation zone attributable to the surrounding buildings. Additionally, the street-network model SIRANE (Soulhac et al., 2011) has also been developed to represent pollutant dispersion within dense

urban canopy. This model assumes that pollutant concentrations are uniform along each street section but explicitly represents the pollutant transfer via street intersection. The dispersion above roof level is handled by a Gaussian plume model. The Model of Urban Network of Intersecting Canyons and Highways, MUNICH (Kim et al., 2018), also uses an explicit representation of street sections, but the dispersion above roof level can be treated with an eulerian approach, by coupling to a chemistry-transport model.

The aforementioned approaches use simplified chemical mechanisms to represent the formation and evolution of atmospheric pollutants. The use of Gaussian plume model indeed implies a stationary assumption which is not compatible with the modelling of complex physico-chemical transformations. This may be a source of substantial uncertainties in air-pollution simulations. Particulate matter can be emitted directly but can also appear after a series of complex chemical formation processes (Fuzzi et al., 2015). Thus, more comprehensive chemical modules must be applied for a consistent representation of the gas phase chemistry and the secondary formation of aerosols (condensation/evaporation, coagulation, nucleation). The coupling of models from different scales is an efficient way to represent local pollutant concentrations, especially near roadside sites for  $\text{NO}_x$ ,  $\text{NO}_2$  and  $\text{O}_3$  (Hooyberghs et al., 2022; Hamer et al., 2020; Lugon et al., 2020; Benavides et al., 2019; Karl et al., 2019; Hood et al., 2018; Berchet et al., 2017; Beevers et al., 2012). To be able to represent the formation of secondary gas and particles at local scales, the MUNICH street-network model was coupled to the SSH-aerosol chemistry and aerosol dynamic model (Sartelet et al., 2020), to provide a detailed evolution of primary and secondary aerosols (Lugon et al., 2021; Kim et al., 2022).

The purpose of this paper is to compare two different downscaling methods both using as starting point regional-scale simulations with CHIMERE (Menuet et al., 2021a) driven by meteorological fields derived from the WRF model (Skamarock et al., 2005; Mailler et al., 2017; Briant et al., 2017; Tuccella et al., 2019) at 1 km x 1 km resolution. The first method consists of the subgrid-scale model embedded in CHIMERE (Valari and Menuet, 2010), ~~it~~-which splits the grid-averaged pollutant concentration into a set of source-specific components based on land-use fractions to represent the subgrid-scale area. The other approach is to use the MUNICH model, which requires explicit information on the street sections of the road network, namely the length, the mean width and the mean height of surrounding buildings. Therefore, we are interested in identifying the conditions under which these two approaches provide similar or diverging simulation results. The simulations performed to compare the methods are conducted over greater Paris, and model results are compared against observations at several traffic monitor sites with different characteristics : inside street-canyons, at roundabouts or at open roads not bounded by buildings. The street-network model MUNICH and the Subgrid method of CHIMERE are briefly described in Section 2. The model set-up and input databases for the simulations, with an emphasis on the use of an urban canopy model in WRF, are described in section 3, monitoring data are detailed in Section 3.3. The results of the study are presented in section 4. Section 5 is the conclusion of the comparative study between the two methods.

## 2 Description of the local models

90 Only the main concepts of the two modelling approaches are recalled here. The details of the implementations of the models are provided in Valari and Menut (2010) for the Subgrid method of CHIMERE and in Kim et al. (2018, 2022) and Lugon et al. (2020) for the MUNICH model.

### 2.1 The CHIMERE subgrid-scale method

CHIMERE is a 3D Eulerian model that solves numerically a set of equations which represents the transport and chemical  
95 transformation of several chemical species in the atmosphere. It is a meso-scale model with a horizontal resolution that ranges from 1 km to 100km, corresponding to study areas that may cover an urban agglomeration to an entire hemisphere.

~~Recently, The SSH-aerosol has been integrated in CHIMERE, allowing for model, named after the three models it incorporates - SCRAM (?), SOAP (?), and H2O (Couvidat et al., 2012) - has been recently integrated into CHIMERE. This model provides~~  
a detailed representation of the formation and ~~dynamical~~-dynamic evolution of atmospheric aerosols (Maison et al., 2023;  
100 Wang et al., 2024). Typically, CHIMERE, as all 3D Eulerian models, assumes that surface emissions are homogeneous over each model grid-cell. However, the subgrid-scale model introduced in Valari and Menut (2010) has been implemented in CHIMERE v2020 (Menut et al., 2021b) and accounts for the heterogeneity of surface emissions due to the action of different activity sectors within the same model's grid-cell. The model transfers this emission heterogeneity to concentration variability (Valari and Menut, 2010). In practice the model uses two pieces of information, emissions from different activity sectors and  
105 an area fraction for each model's grid-cell occupied by each sector taken into account. In this study, we separate emissions into two sectors, those from traffic and those from all other sectors. Following the subgrid-scale scheme implemented here, high emissions from roads are condensed over relatively narrow areas (roads), leading to intensified emissions from the traffic sector compared to the grid averaged emission that would have been diluted to the entire grid-cell volume.

Following this approach, the set of transport equations is solved separately for each considered sector. Equation 1 gives the  
110 temporal evolution of the concentration for a given species for each different sub-grid surface :

$$\frac{\partial c_i}{\partial t} = -\nabla \cdot (\mathbf{U} c_i) + \nabla \cdot (\mathbf{K} \nabla c_i) + E_i + R_i + L_i - \frac{(c_i - \bar{c})}{T_{\text{mix}}} \quad (1)$$

$c_i$  is the concentration computed for the  $i^{\text{th}}$  sector and  $\bar{c}$  the grid-averaged concentration in the cell. The terms from left to right represent the advection by the mean wind  $\mathbf{U}$ , the turbulent mixing parametrized by a gradient diffusion hypothesis with  $\mathbf{K}$  a matrix of turbulent diffusion coefficient,  $E_i$  the emissions from the  $i^{\text{th}}$  sector,  $R_i$  the source and loss terms associated to  
115 chemical transformations and  $L_i$  the deposition inside the  $i^{\text{th}}$  subgrid volume. Finally, the last term, accounts for a mixing of concentrations calculated for the different subgrid volumes. The rate of the mixing is controlled by the term  $T_{\text{mix}}$  which is the ratio between a characteristic length (different in every grid-cell for each emitting surface) and the mean local wind speed.

The advantage of this approach is that the full chemical mechanism operates over each subgrid-scale volume, i.e. for each sector specifically considered, leading to subgrid scale concentrations for all model species. The limitation of the approach

120 is that it does not explicitly take into account i) the effect of the buildings on the flow of pollutants and ii) the emission over each road. As a result, the different street sections within a given cell are not treated separately but rather as an average road configuration inside the grid-cell.

## 2.2 The street-network model MUNICH

MUNICH is a street-network model designed for simulating pollutant concentrations on a local scale. To achieve this, the model needs input data such as background pollutant concentrations, meteorological information, and emissions to accurately simulate concentrations within the street network. The street-network is composed of two types of elements, the street segments and the street intersections. Pollutant concentrations are only resolved for street segments and are assumed to be homogeneous inside each one of them. ~~A transport~~ The integration of the mass conservation equation 2 provides the temporal evolution of the concentration for a given species for each different street segment treated as a box model :

$$130 \quad \frac{\partial c_i}{\partial t} = \frac{1}{V_i} (Q_{i,\text{inflow}} + Q_{i,\text{outflow}} + Q_{i,\text{vert}}) + E_i + R_i + L_i \quad (2)$$

$c_i$  is the concentration (in  $\mu\text{g}\cdot\text{m}^{-3}$ ) computed for the  $i^{\text{th}}$  street segment to which are assigned a length ( $L$ ), a mean width ( $W$ ) and a mean buildings' height ( $H$ ) assumed to be the same on both sides of the road. These three characteristics are in meters.  $V_i$  is the volume (in  $\text{m}^{-3}$ ) of this rectangular cuboid street. The mean wind in the street is parallel to the street axis.  $Q_{i,\text{inflow}}$  and  $Q_{i,\text{outflow}}$  (in  $\mu\text{g}\cdot\text{s}^{-1}$ ) are respectively the mass flux entering the street via the upwind intersection and the mass flux leaving the street via the downwind intersection (both in  $\mu\text{g}\cdot\text{s}^{-1}$ ). A double mass balance, for air and pollutants, determined for each intersection, allows to constrain, relying on the concentrations in the others streets connected and the boundary conditions  $c_{\text{bg}}$ , the advective entering flux.  $Q_{i,\text{vert}}$  is the vertical turbulent flux (in  $\mu\text{g}\cdot\text{s}^{-1}$ ) between the background, here corresponding to concentrations simulated by CHIMERE, and the street. In the framework of the one-way coupling strategy applied in this work, as in many previous studies ([Sarica et al., 2023](#); [Wang et al., 2022](#)) (e.g. [Sarica et al., 2023](#); [Wang et al., 2022](#)), the background concentrations ~~(compared to observations in Annex C)~~ are not modified by MUNICH. These simulated background concentrations are evaluated against observations in Appendix D. This comparison shows that CHIMERE is able to provide boundary conditions for MUNICH that are representative of the background concentrations observed.  $E_i$  represents the emissions from traffic,  $R_i$  combines the source and loss terms associated to chemical transformations and  $L_i$  the deposition inside the  $i^{\text{th}}$  street segment (all three in  $\mu\text{g}\cdot\text{m}^{-3}\cdot\text{s}^{-1}$ ). As with the CHIMERE subgrid-scale model, the full chemical mechanism is applied to each street, leading to street scale concentrations for all the species in the model.

Below we recall a few more specific aspects of the MUNICH model parameterisations to highlight i) the influence of the aspect ratio of the street (the ratio of the mean height to the mean width) and ii) the influence of the friction velocity and the atmospheric stability.

The vertical turbulent flux is computed using the boundary condition  $c_{\text{bg}}$  as follows :

$$150 \quad Q_{i,\text{vert}} = q_v L \frac{c_i - c_{\text{bg}}}{\alpha_f} \quad (3)$$

where  $c_{bg}$  is the background concentration (in  $\mu\text{g}\cdot\text{m}^{-3}$ ) and  $\alpha_r = H/W$  represents the aspect ratio of the street. When this parameter  $\alpha_r$  is less than or equal to  $\frac{1}{3}$ , the street is classified as a "wide canyon". For ratios between  $\frac{1}{3}$  and  $\frac{2}{3}$ , it is categorised as an "intermediate street", and if the ratio is greater than  $\frac{2}{3}$ , the street is designated as a "narrow canyon". The parameter  $q_v$  is the vertical transfer coefficient, that corresponds to the following equation :

155 
$$q_v = \sigma_w l_m \tag{4}$$

$\sigma_w$  is the standard deviation of the vertical wind speed, and  $l_m$  is the mixing length determined using the formulation from Wang (2011). Regarding  $\sigma_w$ , which depends on the friction velocity  $u^*$  and atmospheric stability, three distinct parametrizations are employed to compute this variable, each corresponding to a different atmospheric state. In conditions of neutral atmosphere MUNICH follows Soulhac et al. (2011) and Salizzoni et al. (2009), for a stable atmosphere  $\sigma_w$  is computed according to Cambridge Environmental Research Consultants (2001), and finally for unstable atmosphere MUNICH uses the parametrization from Hunt et al. (1988). ~~Finally, the computation of the wind profile within streets is inspired from Wang (2011, 2014). To estimate-~~

160

~~The implementation of the different parameterizations available in MUNICH to determine the average wind speed in a street is detailed in Maison et al. (2022). The first step is to compute the wind speed at roof level, the parametrization of Macdonald et al. (1998) has been used. The implementation of these parametrizations in MUNICH is detailed in Maison et al. (2022) the mean height of the building,  $u_H$ . It can be derived in MUNICH from a representative wind speed above the urban canopy or from the friction velocity  $u_*$ . This second option and the parameterisation of Macdonald et al. (1998) are used in the current work, allowing an estimate of  $u_H$  based on an average vertical profile at the scale of a neighborhood.~~

165

~~Then only the component of the wind in the direction of the street is taken into account to reconstruct the wind vertical profile in the street. It has been represented in the current study following the work of Wang (2011, 2014). Finally the average wind speed in the street is obtained by integrating the chosen wind profile between the soil roughness and the building height.~~

170

### 3 Description of data and models setup

The subsequent section outlines the input data for regional and local modelling, along with their configuration setup. It includes details about the regional domains utilized, the street-network, and their associated emissions, as depicted in Fig. 1.

#### 175 3.1 Regional scale

Regional scale concentrations are simulated with the CHIMERE-WRF coupled system (Menut et al., 2021b, <https://www.lmd.polytechnique.fr/chimere/>), enriched with the implementation of the SSH-aerosol model (Sartelet et al., 2020, <https://sshaerosol.wordpress.com/>). To obtain pollutant concentrations at 1 km x 1 km resolution we use a three-level nesting configurations as shown in Fig. 1 (a). The largest domain (FRA9) covers France with a spatial resolution of 180 9km×9km. The intermediate domain (IDF3) covers part of the north of France centered around the Île-de-France region with

a spatial resolution of  $3\text{ km} \times 3\text{ km}$ . The innermost domain covers the entire Île-de-France region, centered around the Paris city (IDF1) at a spatial resolution of  $1\text{ km} \times 1\text{ km}$ .

Figures/dom\_network.png

**Figure 1.** (a): The three-level nested simulation domains used to calculate background concentrations (CHIMERE) and meteorological fields (WRF). (b): The street network used for MUNICH simulations. The colorbar represents the road aspect ratio (ratio between the mean height and the mean width of the street), (c): Two-months averaged  $\text{NO}_2$  emission flux (February and March 2014) summed across all activity sectors over the CHIMERE IDF1 grid, (d): Two-months averaged  $\text{NO}_2$  traffic emission flux (February and March 2014) on the MUNICH street network with the location of the measurement stations (dots) and the CHIMERE-WRF mesh (grid lines). Traffic stations are in black, background stations are in purple dots.

### 3.1.1 CHIMERE input data

Initial and boundary conditions for the largest CHIMERE domain (FRA9) are taken from the general circulation model LMDz-  
185 INCA (Hourdin et al., 2006) with a horizontal resolution of  $2.5^{\circ} \times 1.27^{\circ}$  and 39 vertical levels. Anthropogenic emissions for the  
two larger domains are computed from the 2014 EMEP (European Monitoring and Evaluating Program) emission inventory,  
with a spatial resolution of  $0.1^{\circ} \times 0.1^{\circ}$ . Anthropogenic emissions for the domain over the Île-de-France region (IDF1) stem  
from the local, bottom-up inventory of 2014 developed and provided by the AIRPARIF air-quality agency of Île-de-France.  
Biogenic emissions are estimated with the MEGAN model (Guenther et al., 2012) embedded in CHIMERE. Meteorological  
190 variables are computed with WRF running simultaneously with CHIMERE without activation of feedback from CHIMERE to  
WRF.

### 3.1.2 WRF model configuration and input data

The WRF model configuration used for this study is shown in table 1. The initial and boundary conditions for the WRF  
simulations come from the National Centers for Environmental Prediction (NCEP) model and the FNL dataset (National  
195 Centers For Environmental Prediction/National Weather Service/NOAA/U.S. Department Of Commerce, 2000).

Time step	adaptative
Vertical grid spacing	33 levels
Top layer	14 hPa
Bottom layer	997 hPa
surface layer	Revised MM5 Monin-Obukhov scheme
land-surface	Unified Noah land-surface model
boundary-layer	YSU scheme
eddy coefficient	horizontal Smagorinsky first order closure

**Table 1.** Main configuration choices of the WRF simulations.

By default, the coupled CHIMERE-WRF model uses the 2004 land use dataset derived from the Moderate Resolution  
Imaging Spectroradiometer (MODIS) with a resolution of 1 km. However, for the current study we used a reclassification of  
the CORINE categories (from CORINE Land Cover data 2018 with a resolution of 250 m) to MODIS-IGBP based on Vogel  
and Afshari (2020). With three distinct urban categories, this dataset provides a finer spatial representation of the heterogeneous  
200 urban area of the Île-de-France region.

This modification is motivated by the use of an urban canopy model, the SLUCM (Kusaka et al., 2001), applied for this  
study in the two inner nests, IDF1 and IDF3 (simulations over the largest FRA9 domain run without it). The use of a urban



canopy model is required to avoid non-realistic extremely low values of the friction velocity ( $u^*$ ), which drives the transfer of mass between the background and the streets in MUNICH (see Equation 3). Very low values of  $u^*$  lead to concentration peaks  
205 in streets with high emissions.

### 3.1.3 Activation of the Urban Canopy Model

WRF provides different surface layer schemes to compute  $u^*$  and exchange coefficients for heat, moisture, and momentum. Among others, we can cite two surface layer schemes: i) the MM5 (fifth generation Pennsylvania State University - National Center for Atmospheric Research Mesoscale Model) scheme and ii) its revised version proposed by Jiménez et al. (2012).  
210 In our simulations, we used the revised MM5 scheme (see table 1), which sets lower limit values for the friction velocity ( $0.001 \text{ m.s}^{-1}$  by Jiménez et al. 2012) than the original MM5 scheme ( $0.1 \text{ m.s}^{-1}$ ) over land surface, in order to apply surface layer formulation capable to cover the full range of atmospheric stabilities.

Figure 2 shows  $u^*$  time-series at a model grid cell in the urban area with and without an urban canopy model. Without the urban canopy model, extremely low values of  $u^*$  are especially observed during the air pollution episode (first half of March  
215 2014), which is not surprising for a meteorological situation characterized by ~~strong~~ highly stable conditions (Dupont et al., 2016). However, these low values may not be ~~physically relevant~~ realistic in urban environments (Liu et al., 2009). Urban canopy models apply urban roughness sublayer corrections to improve Monin–Obukhov similarity theory (Theeuwes et al., 2019) and result in more realistic vertical profiles of wind speed and friction velocity.

Figures/UST\_AUT\_\_\_\_.png

**Figure 2.** Friction velocities simulated by the WRF model during the two weeks of the air pollution episode of March 2014, for one cell in Paris. The blue line represents a simulation with the SLUCM and the orange line a simulation without the SLUCM. Nighttime is represented by the gray background. The upper dot line is the minimum of the blue line, equals to  $0.078 \text{ m.s}^{-1}$ , and the lower dot line is the minimum of the orange line which corresponds to  $0.01 \text{ m.s}^{-1}$

The WRF model provides different urban canopy models to take into account the effects of urban spaces. Through different  
220 geometric and thermal parameters, these models evaluate the surface energy balance and the wind shear in the urban landscapes  
and provide better representations of the transfer of energy and momentum in cities (Wang et al., 2011). Three urban canopy  
models are available in WRF: i) the Single-Layer Urban Canopy Model, SLUCM (Kusaka et al., 2001) ; ii) the Building  
Environment Parameterization (BEP) model (Martilli et al., 2002) and iii) the Building Energy Model, BEM (Salamanca and  
Martilli, 2009). The first one is composed of a single layer, whereas the others correspond to Multi-Layer models. According  
225 to Allen et al. (2010), the total anthropogenic heat flux released by a city can be divided into three components: the metabolic,  
the motorized vehicles, and the building heat emissions. The latter is well modeled by BEP and BEM, however, these models  
do not give the possibility to add other sources of anthropogenic heat like the traffic component that cannot be neglected in  
a large city (Pigeon et al., 2007). Thus, we chose the SLUCM scheme for our simulations, which enables us to increase the  
anthropogenic sensible and/or latent heat flux in order to represent car traffic heat. Nonetheless, the current study does not  
230 consider latent anthropogenic heat flux due to limited literature data on this topic.

The SLUCM scheme requires maximum values of anthropogenic heat fluxes ( $Q_f$ ) for each considered urban category and a  
diurnal variation profile to modulate these fluxes over time. The daily profile of this heat flux is assumed to be constant from day  
to day in the model and a single maximum is assigned for each urban category. In the case of long simulations (at least several  
months), the configuration of this urban canopy model must be changed because the anthropogenic heat flux depends strongly

235 on seasonal temperature variation. For instance, during the summer period, waste heat generated by air conditioning systems strongly impacts urban air temperatures (Salamanca et al., 2015; Tewari et al., 2017). Therefore, two different  $Q_f$  maximums are settled for February and March 2014 according to Sailor et al. (2015) and Allen et al. (2010). Based on data from Sailor et al. (2015) for Paris, which reported a value of  $39.95 \text{ W.m}^{-2}$  for the entire city during winter, we opted for a closely aligned value of  $40 \text{ W.m}^{-2}$  for the urban category "High urban density", representing the predominant urban category in Paris. Following  
240 several trial simulations against measured data, the optimal values for  $Q_f$  were determined for other urban categories, as detailed in Table 2. In particular to avoid a substantial overestimation of concentrations at relevant stations, it became evident that an increase in this maximum value by a factor of 4 was necessary for the "Commercial/Industrial/Transport" category.

As said previously, the total anthropogenic heat flux comes from different sources with potentially different daily profiles. However, in the SLUCM's version used for the current study, we have the possibility to add only one daily profile for each  
245 urban category. The two approaches used to model the pollutant concentrations in the city of Paris are strongly influenced by car emissions. Thus, to depict road traffic as precisely as possible, the diurnal profile of anthropogenic heat flux built for this study is based on the traffic emissions data from the Airparif inventory, which is displayed in Fig. 3.

Furthermore, as in Lian et al. (2018), thanks to the fine spatial resolution of CORINE Land Cover data we calculate the urban fraction for each  $1 \text{ km} \times 1 \text{ km}$  grid cell of the CHIMERE simulation domain. This fraction is used to modulate the  
250 anthropogenic heat flux at each model grid cell when the SLUCM is activated. Indeed, the anthropogenic heat flux computed by the urban canopy model is proportionate to the urban land cover (urban fraction), if this parameter is equal to 1 the entire anthropogenic heat flux settled in the SLUCM is taken into account. Hence, we are able to use a consistent urban canopy model parameterization for the city of Paris.



**Figure 3.** Diurnal profiles of the anthropogenic heat flux in Paris for February and March 2014 constructed from traffic emission data for our study.

Concerning the configuration of the urban landscape geometry, we obtain the building heights and the road widths from the BDTOPO (version 3) database (<https://geoservices.ign.fr/bdtopo>), roof widths follow Kim et al. (2013) and Thouron et al. (2017). The analysis of several test simulations allowed us to find the most suitable geometry configuration for each of the 3 urban categories from CORINE landcover data. All these parameters are presented in Table 2, and the unmentioned parameters are based on Kusaka et al. (2001).

Parameter \ Urban categories	Commercial /Industrial/ Transport	High urban density	Low urban density
Building level (m)	10	13	9
Standard Deviation of roof height (m)	4	4	4
Building width (m)	15	10	15
Road width (m)	30	20	20
Maximum sensible anthropogenic heat flux ( $\text{W}\cdot\text{m}^{-2}$ )	160 (February)/ 155 (March)	40 (February)/ 35 (March)	30 (February)/ 25 (March)

**Table 2.** List of the main options of the UCM configuration.

The downtown Paris area is classified as “High urban density” in the CORINE landcover dataset. The Parisian suburban area is mainly classified as “Low urban density”, and finally, all the other urban areas corresponding to industrial areas, large shopping centers, highways, or railway networks are classified as “Commercial/Industrial/Transport”.

Without the urban canopy model, WRF calculates friction velocities that are often lower to the limit value of  $0.01 \text{ m}\cdot\text{s}^{-1}$ . As mentioned earlier, this leads to unrealistic high concentrations peaks for all the studied pollutants modeled with MUNICH ( $\text{NO}_2$ ,  $\text{PM}_{2.5}$  and  $\text{PM}_{10}$ ). With the SLUCM configuration described in Table 2, the friction velocity remains consistently above  $0.01 \text{ m}\cdot\text{s}^{-1}$  on cells classified as urban areas.

In the context of our investigation, our findings suggest that ~~reducing~~ raising the friction velocity threshold to  $0.1 \text{ m}\cdot\text{s}^{-1}$  within the surface layer scheme effectively mitigates the occurrence of unrealistic peaks in the simulation. However, it is noteworthy that this threshold value is insufficient for accurately representing the elevated pollutant concentrations observed during air pollution episodes. Our study underscores the significance of incorporating an urban model within the Weather Research and Forecasting (WRF) framework, which introduces an additional anthropogenic heat flux. This appears particularly crucial for locations near highways where traffic-related emissions are substantially high.

### 3.1.4 Configuration of the chemistry

The numerical algorithm used in the CHIMERE-subgrid scale and the CHIMERE/MUNICH approaches are not exactly the same, but they lead to same background concentrations. For example, simulated background concentrations for  $PM_{2.5}$  have a correlation greater than 0.99 at every background station and the bias is of the order of  $0.1 \mu g \mu g^{-3}$ . ~~These background concentrations were evaluated by comparing them with observations from the background stations operated by Airparif, as shown in Annex D. About CHIMERE~~ For CHIMERE and MUNICH simulations, a ~~similar same~~ configuration of SSH-aerosol is used ~~at every scale, which is described in 3.2.1. Finally,~~. Both simulations use ~~H<sup>2</sup>O~~ the same chemical module for gas chemistry, the MELCHIOR2 mechanism (Derognat et al., 2003; P.L.Carter, 1990) and the H<sub>2</sub>O (Hydrophilic/Hydrophobic Organics) reduced mechanism (Couvidat et al., 2018) for the SOA (Secondary Organic Aerosol) formation from VOC (Volatile Organic Compounds), and the same chemical module for gas chemistry, the MELCHIOR2 mechanism (Derognat et al., 2003; P.L.Carter, 1990) and the H<sub>2</sub>O (Hydrophilic/Hydrophobic Organics) reduced mechanism (Couvidat et al., 2012). For both models the time integration of the gas-phase chemistry is solved explicitly and is not based on a stationarity assumption, which means that different time scales can be taken into account.

In addition, the time evolution of particulate concentrations in SSH-aerosol takes into account coagulation and condensation/evaporation of aerosols. The latter is modeled based on a thermodynamic equilibrium hypothesis as detailed in Sartelet et al. (2020). For this study, CHIMERE and MUNICH use ten particle size sections with cut-off diameters at : 0.01, 0.022, 0.048, 0.107, 0.235, 0.516, 1.136, 2.5, 5, 10 and ~~40~~  $\mu m$ . We do not account for nucleation in our simulations because we focus our analysis on particle mass concentration indicators, especially  $PM_{2.5}$  which are little sensitive to this process (Sartelet et al., 2022).

## 3.2 Local scale simulation set-up

### 3.2.1 The street-network model MUNICH

The road segments of the street network considered in this study were originally defined by Airparif, the Île-de-France air quality agency. For each road segment, AIRPARIF assigns emission fluxes for the main pollutants emitted by road traffic. To assign mean width and mean buildings' height to each road segment of the network we use the national BDTOPO database (<https://geoservices.ign.fr/bdtopo>). The mean street width is calculated by adding the mean road width (also from the BDTOPO database) and the sidewalk width (public open-source data available at <https://www.data.gouv.fr/fr/datasets/trottoirs-des-rues-de-paris-prs/>). We combined streets that have intersections less than 4.5 meters apart. The final street network comprises 4655 streets and extends over the city of Paris and its nearby suburbs. The minimum building height in the entire network is established at 1 meter.

The emissions assigned to the streets are given as annual totals. We applied average temporal profiles provided by Airparif to obtain hourly fluxes for the period of the study. The period-averaged  $NO_2$  emission fluxes over the road network are shown in Fig. 1d and highlight the busiest roads. On the same map are also shown the monitor sites of the Airparif network (detailed in Section 3.3).

### 3.2.2 The Subgrid method

305 The subgrid-scale model is fully embedded in CHIMERE, and therefore both models share the same configuration. As explained in section 2.1, grid cells split into several subgrid environments. Here, we split all cells containing a monitoring station into two subgrid environments: "roads", including all emissions from the road network assuming that they are emitted over the grid-cell area fraction corresponding to the road network and "other", including all other emissions assumed to be released over the rest of the grid-cell area. The approach is applied only to cells containing a traffic station, representing a total of 8  
310 cells. Their locations within the grid are illustrated in Figure 1d.

### 3.3 Measurement stations and landuse

Since our goal is to compare two methods that are able to represent pollutant concentrations at street-level scale, we will essentially discuss comparisons at traffic stations (displayed in black in the Fig. 1). Model evaluation focuses on  $\text{NO}_x$ ,  $\text{NO}_2$  and  $\text{PM}_{2.5}$  concentrations. Not all stations measure these three pollutants.  $\text{PM}_{2.5}$  observations are only taken at two traffic  
315 stations, AUT and BP\_EST, close to the ring road. The RN2 station is outside the city on a busy road, while the rest are within the city with lower emissions. Two key features of this measurement network should be noted:

- BP\_EST and SOULT are situated within the same grid-cell, sharing identical emissions data in the Subgrid approach, thus yielding equivalent results from this method. Same case for the stations HAUS and OPERA.
- BASCH and OPERA are two stations situated on a roundabout. Assigning a specific street to these stations is not feasible.  
320 Some results are however discussed in 4.1.2.

The pixels in the CORINE land cover database around the station AUT were originally assigned to the category "*Cropland/natural vegetation mosaïc*" due to their proximity with the Bois de Boulogne public park. However, this observation site is much more influenced by the vicinity of a road junction and the ring road. It was therefore decided to modify the category assigned to the pixel containing the site to "*Commercial/Industrial/Transport*". The modification significantly enhanced the  
325 results of the MUNICH local model simulation for this site. Prior to this correction, MUNICH generated peaks of  $\text{NO}_x$  approaching almost  $4,500 \mu\text{g}\cdot\text{m}^{-3}$  and peaks of fine particles exceeding  $800 \mu\text{g}\cdot\text{m}^{-3}$ , results that were deemed unrealistic. Notably, all stations, except AUT and RN2, are situated within model grid cells categorized as "*high urban density*" according to the CORINE urban classification (detailed in 3.1.3). AUT and RN2 are located within a model grid cell classified as "*Commercial/Industrial/Transport*".

Station	Length (m)	$\alpha_r$	Close ring road	Urban category (from Corine database)	Urban fraction
BP_EST	723	0.09	Yes	High urban density	1.0
AUT	51	0.03	Yes	Commercial/Industrial /Transport	0.97
RN2	219	0.57	No	Commercial/Industrial /Transport	1.0
SOULT	1008	0.44	No	High urban density	1.0
CELES	209	0.81	No	High urban density	0.95
ELYS	302	0.15	No	High urban density	0.96
HAUS	316	0.8	No	High urban density	1.0
BONAP	452	1.48	No	High urban density	0.92
OPERA	n.a	n.a	No	High urban density	1.0
BASCH	n.a	n.a	No	High urban density	1.0

**Table 3.** Characteristics of traffic proximity sites in the Airparif observation network.

## 330 4 Analysis of the simulated local concentrations

The concentrations of  $\text{NO}_x$ ,  $\text{NO}_2$ , and  $\text{PM}_{2.5}$  simulated with MUNICH and the Subgrid method are compared with observations from measurement stations characterized by very dense traffic (BP\_EST, AUT, and RN2) and from stations located inside the city (CELES, ELYS, HAUS, BONAP, SOULT), where pollutant emissions from traffic are lower. For these stations, we analyze the impact of i) differentiating emissions and aspect ratios (H/W); ii) the daily concentration profile for each approach. The specific case of stations BASCH and OPERA are discussed independently in section 4.1.2.

### 4.1 Evaluation against observations at traffic sites

#### 4.1.1 Global analysis

Model evaluation involves comparing the simulated concentrations with the observations through various statistical metrics that we deemed relevant to our analyses : the fractional biases (FB), the Pearson correlation (R) and the Normalized mean square error (NMSE), that are described in the [Annex-Appendix A](#). The comparisons are done for hourly concentrations and for the entire simulation period. Table 4 shows model scores for  $\text{NO}_x$ ,  $\text{NO}_2$  and  $\text{PM}_{2.5}$  concentrations simulated with the two modelling methods.

For  $\text{NO}_x$  concentrations, the fractional bias (FB) varies from -0.22 (RN2) to 0.09 (BP\_EST) with MUNICH and from -1.06 (AUT) to 0.35 (SOULT) with the Subgrid method. The average of the FB on the measurement network studied (8 stations)

345 is equal to -0.07 for MUNICH and -0.35 for the Subgrid method. For the two stations on the Parisian ring road (BP\_EST and AUT), the Subgrid approach significantly underestimates the concentrations with a FB of around -0.84. We observed that the Subgrid method significantly overestimates NO<sub>x</sub> concentrations at the SOULT station. An overarching problem with the description of emissions arises due to the heterogeneity between SOULT and BP\_EST, located in the same cell. [Indeed, this area is crossed by the heavily trafficked Paris ring road, which introduces significant urban spatial heterogeneity \(see Figure 4\).](#)

350 This is extensively discussed in Section 4.2. The street-network model gives in general better performances than the Subgrid method for NO<sub>x</sub>. The correlation coefficient remains an exception, as both methods exhibit nearly identical performance, around 0.62.

For NO<sub>2</sub> concentrations, the fractional bias (FB) varies from -0.1 (AUT) to 0.24 (BP\_EST) with MUNICH and from -0.62 (AUT) to 0.34 (SOULT) with the Subgrid method. The average of the FB on the measurement network studied is equal to 0.08

355 for MUNICH and -0.07 for the Subgrid method. In contrast to NO<sub>x</sub> concentrations, MUNICH demonstrates an improvement in the correlation of approximately 8% compared to the Subgrid approach. The average correlation for the street-network model is 0.67, while it is 0.59 for the Subgrid method. We also noted that for NO<sub>2</sub> and NO<sub>x</sub> concentrations, the street-network model generates lower NMSE for most of the stations studied. The superior performance of the Subgrid method for NO<sub>2</sub> compared to NO<sub>x</sub> in terms of fractional bias is apparent. This distinction may be attributed to the regional component of NO<sub>2</sub> being more

360 prominent than that of NO<sub>x</sub>, which is more influenced by local traffic emissions.



**Figure 4.** [The grid-cell that contains the stations BP\\_EST and SOULT, displayed with BDTOPO database: buildings are represented in grey, the open street in blue, the intermediate street in yellow, and the canyon street in purple.](#)

The statistical analysis for PM<sub>2.5</sub> is conducted solely on two stations situated along the Parisian ring road (refer to Table 4). It is evident that MUNICH significantly outperforms the Subgrid approach for these two specific stations, albeit not in terms



of correlation. The Subgrid method achieves an average correlation of 0.8, while MUNICH exhibits an average correlation of approximately 0.7 for the two stations. To complete this overview of the performances of each method, the summary of the criteria results from Herring and Huq (2018) for all the stations studied is shown in [Annex-Appendix C](#).

		NO <sub>x</sub>			NO <sub>2</sub>			PM <sub>2.5</sub>		
		FB	R	NMSE	FB	R	NMSE	FB	R	NMSE
<b>BP_EST</b>	Subgrid	-0.62	<b>0.56</b>	1.21	<b>-0.16</b>	0.52	<b>0.29</b>	-0.49	<b>0.75</b>	0.85
	MUNICH	<b>0.09</b>	0.47	<b>0.55</b>	0.24	0.52	0.31	<b>-0.02</b>	0.64	<b>0.51</b>
<b>AUT</b>	Subgrid	-1.06	0.61	2.46	-0.62	0.59	0.64	-0.61	<b>0.85</b>	1.08
	MUNICH	<b>-0.18</b>	<b>0.64</b>	<b>0.4</b>	<b>-0.1</b>	<b>0.67</b>	<b>0.2</b>	<b>-0.1</b>	0.77	<b>0.44</b>
<b>RN2</b>	Subgrid	-0.38	<b>0.64</b>	0.68	-0.15	0.57	0.2	-	-	-
	MUNICH	<b>-0.22</b>	0.63	<b>0.48</b>	<b>-0.05</b>	<b>0.65</b>	<b>0.13</b>	-	-	-
<b>SOULT</b>	Subgrid	0.35	0.63	0.74	0.34	0.64	0.37	-	-	-
	MUNICH	<b>0.01</b>	<b>0.64</b>	0.74	<b>0.17</b>	<b>0.75</b>	<b>0.14</b>	-	-	-
<b>CELES</b>	Subgrid	-0.27	<b>0.69</b>	0.74	<b>0.02</b>	0.64	0.24	-	-	-
	MUNICH	<b>0.05</b>	0.68	<b>0.48</b>	0.19	<b>0.71</b>	<b>0.18</b>	-	-	-
<b>ELYS</b>	Subgrid	-0.21	0.56	0.45	<b>0.02</b>	0.56	0.19	-	-	-
	MUNICH	<b>0.02</b>	<b>0.57</b>	<b>0.35</b>	0.13	<b>0.68</b>	<b>0.12</b>	-	-	-
<b>HAUS</b>	Subgrid	-0.29	0.6	0.49	-0.06	0.57	0.2	-	-	-
	MUNICH	<b>-0.17</b>	<b>0.65</b>	<b>0.34</b>	<b>0.01</b>	<b>0.7</b>	<b>0.1</b>	-	-	-
<b>BONAP</b>	Subgrid	-0.35	0.67	0.52	<b>0.004</b>	0.66	0.2	-	-	-
	MUNICH	<b>-0.17</b>	<b>0.71</b>	<b>0.32</b>	0.11	<b>0.74</b>	<b>0.1</b>	-	-	-

**Table 4.** Statistical indicators for comparison of hourly concentrations of NO<sub>x</sub>, NO<sub>2</sub> and PM<sub>2.5</sub> from February to March 2014 at traffic stations. Bold numbers indicate the best performance.

The two-month period under study includes a pollution episode from March 5 to 17. When comparing the fractional bias and the NMSE of each method across different periods (during the pollution episode and outside it), no significant differences are observed between the two approaches for the three pollutants analysed. The NMSE remains consistent throughout the entire period, and the fractional bias observed outside the air pollution episode is fairly similar to that calculated during the pollution episode (see Table C3 in Appendix C).

#### 4.1.2 Analysis specific to stations

A substantial gas concentration disparity between the two approaches is evident throughout the entire period for AUT (see Fig. 5) and BP\_EST. This pattern is also observed in PM<sub>2.5</sub> concentrations. Notably, these are the only two stations in the

measurement network located on the heavily trafficked Parisian ring road. The Subgrid method provides concentrations at  
375 street level, but on average for an entire cell of 1 km x 1 km. The result provided by the Subgrid method should therefore be  
interpreted as an average on-road concentration for the different street segments located inside the grid cell. Considering for  
instance the grid cell containing the BP\_EST station, the Subgrid method uses a single NO<sub>2</sub> emission flux of 5.7  $\mu\text{g}\cdot\text{s}^{-1}\cdot\text{m}^{-2}$   
in average over the simulation period, representing a spatially averaged flux among all road segments located inside the grid  
cell. The NO<sub>2</sub> emission flux for the road segment containing the BP\_EST station, explicitly provided to MUNICH, is estimated  
380 equal to 18.8  $\mu\text{g}\cdot\text{s}^{-1}\cdot\text{m}^{-2}$ . It is therefore not surprising that the concentration simulated with the Subgrid method underesti-  
mates concentrations at the BP\_EST station. Symmetrically, the common NO<sub>2</sub> emission flux used by the Subgrid method for  
the SOULT station, located in the same grid cell than BP\_EST, overestimate the one given for the street containing this sta-  
tion, equal to 2.49  $\mu\text{g}\cdot\text{s}^{-1}\cdot\text{m}^{-2}$ . An overestimation of the concentrations can therefore be expected. This a priori qualitative  
[analyzeanalysis](#), also valid for NO<sub>x</sub> and PM<sub>2.5</sub> emission fluxes, appears confirmed by the comparison between concentrations  
385 simulated by the Subgrid method and observations, particularly for NO<sub>x</sub> : At the BP\_EST station, the fractional bias (FB)  
stands at -0.62, and at SOULT, it equals 0.35. A similar trend is noted for NO<sub>2</sub>, albeit less pronounced at BP\_EST, with an FB  
of -0.16, and still evident at SOULT with an FB of 0.34. While observation data for fine particles on SOULT are unavailable,  
simulations for BP\_EST indicate an underestimation with a FB of 0.49.

For the other stations within the city, the differences between the two approaches are less noticeable. The simulated con-  
390 centrations generated by each method appear nearly identical for stations such as HAUS and BONAP (the former station is  
depicted in Fig. 5). However, the discrepancies are slightly more important on CELES and ELYS. About NO<sub>x</sub> concentrations,  
MUNICH performs better than the Subgrid method on these two stations throughout the entire period studied (see Table 4),  
but this is not the case for NO<sub>2</sub>. CELES, located on the docks, is associated with a cell characterized by higher emission het-  
erogeneity, which could contribute to the observed disparities between the approaches. In the case of ELYS, the station shares  
395 similarities in terms of traffic emissions with HAUS and BONAP. However, a crucial distinction lies in its aspect ratio, which  
is significantly lower (as detailed in Section 3). The impact of this aspect ratio on the observed discrepancies is described in  
Section 4.2.

As mentioned above, the OPERA and BASCH measurement stations are located on roundabouts. The primary challenge  
in simulating pollutant concentrations at these stations comes from the uncertainty associated with the estimation of traffic  
400 emissions. Noticeably, the local [queuing-congestion](#) effects and the shutdowns and restarts that this entails are not explicitly  
taken into account to build the emission inventory. Consequently, there is a potential underestimation of traffic emissions at  
these locations. To further characterise this issue concerning MUNICH, we conducted an analysis of each street connected to  
one of these roundabouts, identifying two streets: one yielding the best statistical indicators and another producing the worst.  
The table 5 showcasing significant fractional biases for each approach at the two stations. For OPERA, the performance of the  
405 Subgrid approach falls between the street with the best results (MUNICH\_1 in Table 5) and the one with the least accurate  
gas concentration (MUNICH\_2). However, a different scenario unfolds for BASCH, where the Subgrid method performs even  
worse than the street generating the least accurate results. The main distinction between these two cells lies in the fact that the  
urban environment surrounding OPERA is more homogeneous than that surrounding BASCH.

		NO <sub>x</sub>			NO <sub>2</sub>		
		FB	R	NMSE	FB	R	NMSE
	Subgrid	-0.98	0.64	1.86	-0.5	0.62	0.46
BASCH	MUNICH_1	-0.69	0.73	0.88	-0.29	0.76	0.18
	MUNICH_2	-0.91	0.71	1.52	-0.43	0.76	0.31
	Subgrid	-0.72	0.57	1.01	-0.31	0.53	0.29
OPERA	MUNICH_1	-0.61	0.59	0.76	-0.26	0.64	0.19
	MUNICH_2	-0.75	0.54	1.11	-0.36	0.57	0.29

**Table 5.** Statistical indicators for comparison of hourly concentrations of NO<sub>x</sub>, NO<sub>2</sub> and PM<sub>2.5</sub> from February to March 2014 at traffic stations on a roundabout. MUNICH\_1 represents the street providing the most accurate estimations of concentrations among the streets connected to the associated roundabout, while MUNICH\_2 corresponds to the street with the least accurate gas concentration estimations.

Through this first analysis, it becomes clear that the disparities between the approaches vary greatly depending on the location of the stations. These latter are characterised by different emissions and different types of buildings. These aspects are further explored in the subsequent sections, ~~starting with a discussion on emissions.~~

Figures/serie10\_temp\_byday.png

**Figure 5.** Daily average concentrations observed (black dot), simulated by MUNICH (in orange) and by the Subgrid method (in blue) over two months, at some of the most representative stations in the Airparif measurement network, for  $\text{NO}_x$ ,  $\text{NO}_2$  and  $\text{PM}_{2.5}$  concentrations.

#### **4.2 Impact of differentiated emissions and aspect ratio**

The case of stations BP\_EST and SOULT, both located inside the same grid cell, illustrates an expected limitation of the Subgrid method in comparison to MUNICH. The BP\_EST station is located on the heavily trafficked Paris ring road, while the SOULT station is on a much less busy boulevard, further away from the highway. The presence of a highway traversing this cell introduces significant urban spatial heterogeneity (refer to Fig. 4).

The grid cell that contains the stations BP\_EST and SOULT, displayed with BDTOPO database: buildings are represented in grey, the open street in blue, the intermediate street in yellow, and the canyon street in purple.

By definition, the Subgrid method is supposed to represent a portion of a neighborhood, whereas the MUNICH model generates concentrations for every single street. To emphasize the impact of this conceptual difference, in Fig. 6, we compare the concentrations simulated with MUNICH for each street to the corresponding CHIMERE/Subgrid grid cell (area of 1 km<sup>2</sup>), but also with the mean of all the streets of the MUNICH road network located inside this CHIMERE grid cell. This new averaged MUNICH output is noted as MUNICH\_cell in Fig. 6. The fractional bias generated by [MUNICH\_cell - Subgrid] (depicted by the blue barplot) is significantly lower than that of [MUNICH - Subgrid] (green barplot) at all stations for each pollutant. This outcome underscores the similarity in the average behaviour of each method.

Figures/diff\_meth\_3barplot.png

**Figure 6.** Comparison of the fractional biases between MUNICH and the Subgrid method (in green) and between the mean of all the street segments computed by MUNICH inside the cell (MUNICH\_cell) and the Subgrid method (in dark blue) for concentrations of  $\text{NO}_x$ ,  $\text{NO}_2$  and  $\text{PM}_{2.5}$  for each traffic stations. The stations are ordered from left to right, from the station with the highest  $\text{NO}_2$  emissions (BP\_EST) to the station with the lowest  $\text{NO}_2$  emissions (BONAP). Below the figure of the middle is displayed the  $\text{NO}_2$  mean emission (in  $\mu\text{g}\cdot\text{s}^{-1}\cdot\text{m}^{-2}$ ) over the two months studied. Above the figure at the top, the aspect ratio of associated to each station is indicated: in blue the stations are located in a wide street, in yellow in an intermediate street, and in purple inside a narrow canyon.

Cells Stations located in cells intersected by the Parisian ring road exhibit the most substantial ~~fractional biases (FB)~~ difference between the two approaches for  $\text{NO}_x$ ,  $\text{NO}_2$ , and  $\text{PM}_{2.5}$ . Additionally, when examining AUT and RN2, two stations with close-comparable emissions ( $13.3\mu\text{g}\cdot\text{s}^{-1}\cdot\text{m}^{-2}$  and  $11.0\mu\text{g}\cdot\text{s}^{-1}\cdot\text{m}^{-2}$  respectively), their FB significantly differs for the three pollutants. ~~This indicates that the~~ The observed discrepancies are then not solely attributable to traffic emission

430 levels. As anticipated from the statistics in 4, discrepancies between the two approaches appear more pronounced for  $\text{NO}_x$  estimations than for  $\text{NO}_2$ .

Notably, Fig. 6 highlights a significant observation: the fractional bias generated by MUNICH\_cell-Subgrid (depicted by the blue barplot) is significantly lower than that of MUNICH-Subgrid (green barplot) at all stations for each pollutant. This outcome underscores the similarity in the average behaviour of each method and justifies the performance disparities as a consequence of urban heterogeneity tied to emissions and urban topography.

It is interesting to quantify the influence of these two factors separately on the differences observed. However, it's worth noting that these two factors they are not entirely independent: in our domain, a highway with substantial traffic emissions generally corresponds to a broad and open road. Moreover, in MUNICH, in MUNICH, the impact of the aspect ratio  $\alpha_r$  on street concentrations is more visible for street-pronounced for streets with high emissions than for street-those with low emissions.

440 Figure B1 shows the between our two approaches for  $\text{NO}_x$  on all the streets inside two chosen cells, depending on the aspect ratio on x-axis, and the mean of the emissions on y-axis. The results displayed in this figure confirmed the strong correlation between the emissions and the disparities observed between MUNICH and the Subgrid method.

Bias between MUNICH and the Subgrid method for  $\text{NO}_x$ , as a function of the  $\alpha_r$  (X axis) and the average emissions of MUNICH (Y axis, in  $\mu\text{g}\cdot\text{s}^{-1}\cdot\text{m}^{-2}$ ) of all the streets (point) of a cell, over February and March 2014. The left panel shows the results for the cell containing stations BP\_EST and SOULT, the right one for the cell containing HAUS.

The impact of emission heterogeneity on model discrepancies is clearly observed by comparing the two panels of Fig. B1. The cell containing a part of the Paris ring road, leading to a wide range of emission values, presents a significantly greater range of bias values than the cell inside the city (the scatter plot of the right in Fig. B1). Indeed, we observed that for stations near the Paris ring road, namely BP\_EST, AUT, and RN2, the minimum fractional bias averages at -0.61, while the maximum reaches 1.08. In contrast, for stations within the city, the fractional bias ranges between -0.29 and 0.53 on average. This observation confirms that the discrepancies. Additionally, a third factor could impact these discrepancies. Because the Subgrid method has information only about the street area, we could expect some contribution from the wind direction. Its influence on the discrepancies observed between the approaches are significantly less pronounced in areas with a more homogeneous distribution of emissions compared to those adjacent to highways, which introduce heterogeneous emissions. has been studied and does not reveal any significant impact in our case. But this could be due to the fact that the wind direction barely changes over the studied period, making it challenging to analyze its influence.

The Spearman's rank correlation coefficient (defined in A) between 1) the FBs in the mean concentrations (for the two months studied) calculated by the two approaches and 2) the differences,  $E_{\text{diff}}(i)$ , between the local emission in street  $i$  ( $E_i$ ) and the average of emissions over the  $N_s$ . As expected, through an extension of the analyze on all the streets in the corresponding cell (weighted by street surfaces  $\{S_j\}_{j=1, N_s}$ ) is used to quantify the strength of the relationship.  $E_{\text{diff}}(i)$  is then defined as:

$$E_{\text{diff}}(i) = E_i - \frac{\sum_{j=1, N_s} E_j S_j}{\sum_{k=1, N_s} S_k}$$

For  $\text{NO}_x$ ,  $\text{NO}_2$ , and  $\text{PM}_{2.5}$ , the coefficients are 0.88, 0.85, and 0.87, respectively. These values confirm a significant correlation (potentially non-linear) between the emission heterogeneity and the observed disparities between the modelling approaches.

465 cells calculated by the Subgrid method (see Appendix B), it is easy to show that emission heterogeneities is an important factor in the discrepancies observed between the two approaches. ~~The other cell illustrated in Fig. B1, which include HAUS station, represents an area with more homogeneous emissions. In this type of urban area (such as the cells containing ELYS and BONAP),~~ However, as observed in Figure B1 (b), comparing concentration differences with the aspect ratio of the impact of emission heterogeneity is less prominent but the influence of street aspect ratio on the differences observed between the two  
470 methods remains difficult to discern. We made the same observation for  $\text{NO}_2$  and  $\text{PM}_{2.5}$ .

Comparing concentration differences with street, the aspect ratio seems not very relevant. This can be explained by the absence of a direct use of the aspect ratio ~~of the street is less relevant as this variable is not directly used~~ in the Subgrid approach, which only considers the surface area of the street.

Consequently, further data is required to ascertain the impact of street aspect ratios on the differences observed between the  
475 two approaches. We conducted four additional MUNICH simulations, each with an identical aspect ratio for the entire street network: one with  $\alpha_r=0.25$ , another with  $\alpha_r=0.5$ , a third with  $\alpha_r=1.0$ , and a fourth with  $\alpha_r=1.5$ . These values are chosen to cover the range of cases observed in our network. The heights and widths of the streets have been resized to maintain their volume following Kim et al. (2022). Figure 7 presents the results of these investigations and underscores the importance of  $\alpha_r$ .



**Figure 7.** Bias between four MUNICH simulations with identical  $\alpha_r$  and the Subgrid method for  $\text{NO}_x$  as a function of the  $\alpha_r$  (X axis) and the average emissions of MUNICH (The y-axis, without units, corresponds to the streets ranked in ascending order of emissions) of all the streets (point) of all the cells calculated by the Subgrid method, on February and March 2014.



It logically shows that for a given emission level, the FB between MUNICH and the Subgrid method increases with  $\alpha_r$  due to the increase of MUNICH concentrations. However, this increase is very limited for the streets with low emissions (below  $\sim 1 \mu\text{g}\mu\text{g}\cdot\text{s}^{-1}\cdot\text{m}^{-2}$ ) since for such streets the concentration level is mainly driven by background concentrations.

About  $\text{NO}_x$ , the MUNICH simulation with the highest  $\alpha_r$  (1.5) yields higher concentrations than the Subgrid method for most streets, while the opposite behaviour is observed for the MUNICH simulation with the lowest  $\alpha_r$  (0.25). The average biases over the streets between the Subgrid method and the different MUNICH simulations are  $5 \mu\text{g}\mu\text{g}\cdot\text{m}^{-3}$ ,  $34 \mu\text{g}\mu\text{g}\cdot\text{m}^{-3}$ ,  $92 \mu\text{g}\mu\text{g}\cdot\text{m}^{-3}$  and  $153 \mu\text{g}\mu\text{g}\cdot\text{m}^{-3}$  for  $\alpha_r$  respectively equal to 0.25, 0.5, 1.0 and 1.5. The same trend on average biases is observed for  $\text{NO}_2$  and  $\text{PM}_{2.5}$ , with values ranging from  $3 \mu\text{g}\mu\text{g}\cdot\text{m}^{-3}$  with  $\alpha_r=0.25$  to  $37 \mu\text{g}\mu\text{g}\cdot\text{m}^{-3}$  with  $\alpha_r=1.5$  for  $\text{NO}_2$  and from  $0.7 \mu\text{g}\mu\text{g}\cdot\text{m}^{-3}$  to  $8 \mu\text{g}\mu\text{g}\cdot\text{m}^{-3}$  for  $\text{PM}_{2.5}$ .

~~We observe that the~~ The MUNICH simulation with  $\alpha_r = 0.25$  closely mirrors the Subgrid simulation for  $\text{NO}_x$  that can be approximately considered as a passive tracer with a linear behaviour with respect to emissions. Both simulations rely on the same total traffic emissions, with only their spatial distribution changing. In other words, this simulation most accurately replicates the average dispersion conditions observed with the Subgrid method compared to the other simulations conducted.

Following this observation, the biases between the Subgrid simulation and MUNICH simulation with  $\alpha_r = 0.25$ , can be used to approximately assess the influence of the representation of emission heterogeneity in the difference between the two methods. The biases range from -39 to  $122 \mu\text{g}\mu\text{g}\cdot\text{m}^{-3}$ , with a standard deviation equal to  $17 \mu\text{g}\mu\text{g}\cdot\text{m}^{-3}$  for cells within the city. However we notice that for cells with heterogeneous emissions (including highways), this standard deviation is clearly higher ( $170 \mu\text{g}\mu\text{g}\cdot\text{m}^{-3}$ ), with biases ranging from -82 to  $922 \mu\text{g}\mu\text{g}\cdot\text{m}^{-3}$ .

If we carry out the same analysis but instead of using the Subgrid simulation, we compute the bias between the original MUNICH simulation and the one with  $\alpha_r = 0.25$ , we can then approximately assess the impact of the aspect ratio. For cells within the city, we obtain a standard deviation of  $21 \mu\text{g}\mu\text{g}\cdot\text{m}^{-3}$ , with values ranging from -152 to  $89 \mu\text{g}\mu\text{g}\cdot\text{m}^{-3}$ . Once again, the biases computed for cells intersected by highways are generally higher, with a standard deviation reaching  $93 \mu\text{g}\mu\text{g}\cdot\text{m}^{-3}$ , ranging from -152 to  $386 \mu\text{g}\mu\text{g}\cdot\text{m}^{-3}$ .

Firstly, we noticed that the influence of both the aspect ratio and emission heterogeneities are more pronounced on cells intersected by highways. Secondly, although their impacts are fairly equivalent on city centre cells, we observed about the cells intersected by highways that the impact of emission heterogeneity is considerably more significant than that of the aspect ratio. This is reflected in the standard deviation, which is almost twice as large for the influence of emissions compared to the aspect ratio.

The previous analysis performed on  $\text{NO}_x$  cannot be directly extended to  $\text{NO}_2$  and  $\text{PM}_{2.5}$  due to the non-linearity of the chemistry and its impact on the secondary contribution to the concentrations. Within the comparison between the Subgrid method and the four different MUNICH simulations with constant  $\alpha_r$ , the relative variation of simulated concentrations is greater in the case of  $\text{NO}_x$  than for  $\text{NO}_2$  and  $\text{PM}_{2.5}$ . For instance, the fractional bias between the original MUNICH simulation and the one with  $\alpha_r = 0.25$  varies from -0.7 to 1.5. In comparison, the corresponding fractional bias for  $\text{NO}_2$  and  $\text{PM}_{2.5}$  ranges from -0.2 to 1.1. The  $\text{NO}_2$  and  $\text{PM}_{2.5}$  concentrations calculated by MUNICH are less affected by the street aspect ratio because

the concentrations of these pollutants have a more significant background component compared with  $\text{NO}_x$ , whose concentration spatial patterns are more marked by road traffic emissions.

515 The influence of the local description of emissions is undoubtedly very important in the difference of performances of the two models studied, especially on highways where the Subgrid method is not capable of using sufficiently accurate emissions. About the aspect ratio of the street, its impact on the disparities observed between each method is lower but present.

### 4.3 Analysis of daily cycles

The aspect ratio of the street and emission play an important role in the differences observed between the approaches. Nevertheless, the impact of these factors may vary depending on the specific time periods under analysis. The subsequent section delves into the distinctions observed throughout different times of the day.

In Fig. 8, two-month averaged 24-hour profiles of the bias between observed and simulated concentrations for  $\text{NO}_x$  and  $\text{NO}_2$  at AUT, HAUS and BONAP stations are presented. The central horizontal bar in the boxplots represent the median of all the biases during the two months for a specific hour. The other horizontal bars represent the different quartiles. These three measurement stations have been selected to represent various cases highlighted in the previous section: AUT is situated in an urban zone characterised by a significant emission heterogeneity, HAUS is located in an area with more homogeneous emissions, and finally, BONAP shares similarities with HAUS but is positioned on a street notably narrowest than other ones around.

~~About the station AUT. In areas with significant emission heterogeneity (such as AUT and BP\_EST), the Subgrid approach underestimates the gas concentrations at each hour of the day unlike the street network model, an area with an area characterized by significant emission heterogeneity. This underestimation is especially, with the discrepancies compared to MUNICH being particularly marked during the concentration peaks corresponding to the rush hours (from 5 am to 9 am and from 5 pm to 8 pm). It's also at these moments that the discrepancies between the two approaches are more pronounced. This is also true. This pattern is also observed for  $\text{PM}_{2.5}$  concentrations. The behaviour is different for stations located in In areas with less emission heterogeneity (HAUS and BONAP). In these cases, the two methods exhibit alternating periods of over- and under-estimation of  $\text{NO}_x$  and  $\text{NO}_2$  concentrations throughout the day, and with the dispersion of the bias of each approach is being quite similar. Specifically, the spreads of these biases (the difference between the maximum and minimum bias) for the two methods remain fairly similar for a given hour of the day. This underscores the similarity in the daily variability of the methods. The other stations are displayed in Appendix E.~~

540 ~~The Fig. 9 illustrates~~

~~Figure 9 shows the averaged 24-hour profiles of the bias between MUNICH and the Subgrid approach at each hour of the day for the same three stations. It confirms that the differences are more pronounced during the daylight, and the significant influence of the emission heterogeneity (BP\_EST has the same behavior as AUT). The  $\text{NO}_x$  bias at BONAP station slightly exceeds that of HAUS, possibly attributable to the effect of  $\alpha_r$ , given that the street, where the BONAP is localated, is among the narrowest in its urban area.~~

However, ~~illustrates that the~~ discrepancies between the two approaches become more pronounced at certain times of the day. These differences are minimal during nighttime and escalate with traffic. Regarding NO<sub>x</sub> concentrations, the bias between the two methods remains positive and increases slightly throughout daylight hours. This indicates that for these streets, MUNICH retains traffic emissions for longer than ~~Subgrid~~ the Subgrid approach. Conversely, for NO<sub>2</sub> concentrations, the sign of the bias varies ~~along throughout~~ the day. ~~Indeed, while~~ While in most cases the street-network model generates higher concentrations of NO<sub>2</sub> than the Subgrid method, ~~this the~~ latter generates higher concentrations during the morning. ~~Note~~ It is noteworthy that all the other stations (apart from AUT and BP\_EST) behave in the same way as HAUS and BONAP, ~~which are as~~ shown in Fig. 9.

At the end of the night, the O<sub>3</sub> concentrations of the Subgrid are higher than those of MUNICH. This appears consistent with higher exchange between these streets and the background environment in the Subgrid method ( $\alpha_r \sim 0.25$ ) compared to MUNICH. The peak in morning traffic emission starts to bring NO<sub>x</sub> while the atmospheric boundary layer is not fully developed, the titration of O<sub>3</sub> by NO then leads to higher NO<sub>2</sub> chemical production in the Subgrid method. Around 7:00am (local hour), the O<sub>3</sub> concentrations are very similar in both models, but the development of the boundary layer then brings more O<sub>3</sub> in the Subgrid method. This allows the chemistry production of NO<sub>2</sub> to overcompensate during some hours the greater dilution of the Subgrid method.

The daily profiles confirm that the representation of emission heterogeneity is the main factor contributing to the differences observed between the two models. These differences are more pronounced during the daylight and may vary depending on the moment of the day.

Figures/all\_boxplot\_byday.png

**Figure 8.** Daily profiles of the bias (in  $\mu\text{g}\cdot\text{m}^{-3}$ ) between observed and simulated concentrations for the period of February-March 2014, for  $\text{NO}_x$  and  $\text{NO}_2$  concentrations.

Figures/2\_day\_fb.png

**Figure 9.** Daily profiles of the bias (in  $\mu\text{g}\cdot\text{m}^{-3}$ ) between MUNICH and Subgrid simulations over the period of February-March 2014, for  $\text{NO}_x$  and  $\text{NO}_2$  concentrations.

## 5 Conclusions

565 In the current paper, we compared two methods to simulate street-level pollutant concentrations of  $\text{NO}_x$ ,  $\text{NO}_2$ , and  $\text{PM}_{2.5}$  with observations at traffic measurement stations. The simulations are performed over Paris during a winter period, February and March 2014. The first approach, the Subgrid method, is a statistical method capable of disaggregating emissions of different sectors (traffic, residential, park ...) inside a grid cell. In our case, we subdivide the cells where there are traffic stations into two environments in order to concentrate the traffic emissions on a road surface. The second approach is the MUNICH

570 model, which is based on a street-network approach. The considered network in MUNICH is composed of 4655 streets and represents the city of Paris and its close suburbs. These two methods make use of identical emissions, meteorological data, and background concentrations. An urban canopy model (SLUCM) has been applied in the WRF model to generate the meteorological data used by each method. We integrated three different urban categories and the urban fraction per grid-cell from CORINE land-use database in the geographic data file used by the WRF model. The simulations carried out as part of

575 this study confirm the need to represent the anthropogenic sensible heat flux in the SLUCM for a winter period, that come mainly from traffic, domestic energy and human metabolism. These adjustments significantly influence the friction velocity and improve the background concentration simulated by the CHIMERE model and the performance of MUNICH.

While the street-network approach respects all the strictest criteria on the entire measurement network studied for  $\text{NO}_x$ ,  $\text{NO}_2$ , and  $\text{PM}_{2.5}$ , this is not the case for the Subgrid method. This latter failed to represent correctly gas and fine particle

580 concentrations on stations located in urban area with important spatial or temporal emission heterogeneity. For stations situated

in the city centre of Paris, MUNICH exhibits a lower fractional bias relative to observations (approximately -0.06) for NO<sub>x</sub> concentrations compared to the Subgrid method (-0.28), but the results concerning NO<sub>2</sub> concentrations are more similar.

The most significant differences observed between the two approaches concern cells containing highly trafficked roads. These disparities are not directly attributed to the elevated emissions in these areas but are influenced by the presence of the Parisian Ring road (Highway), which substantially alters the urban landscape, leading to heterogeneous emissions and varying building dimensions. We proposed an analysis of the respective role of emission and topography heterogeneities. Those linked to emissions appear to generate a larger range of bias values between the two methods than those linked to topography in urban area including the Parisian Ring road. In the City centre of Paris, both aspects appear to have a much more similar impact.

The analysis of the daily cycles reveals that the discrepancies between the approaches are more pronounced during rush hours. At the city centre stations, which are characterised by fairly homogeneous emissions, we noted in the morning that the Subgrid method can generate higher NO<sub>2</sub> concentrations than MUNICH due to higher ozone import.

This paper has identified potential areas for improvement in each of the local approaches: the robustness of the street network model could be improved by a better representation of local meteorology, and applying the Subgrid method with a more diverse range of traffic area zones could enhance its performance on cells containing highways. Finally, these results offer encouraging prospects for a potential dynamic coupling between MUNICH and the coupled model CHIMERE-WRF. In a future work, the pollution transfers between local and regional scales will be enhanced through the development of a dynamic coupling (a two-way nesting) between the CHIMERE and MUNICH models.

*Code availability.* The CHIMERE model is available on the website

<https://www.lmd.polytechnique.fr/chimere/> and for download at <https://doi.org/10.14768/8afd9058-909c-4827-94b8-69f05f7bb46d>. The MUNICH v2.0 model is available at <https://doi.org/10.5281/zenodo.6167477> or the git repository at <https://github.com/cerea-lab/munich>

## Appendix A: Definition of the statistical indicators

The subsequent equations present the definitions of the statistical indicators employed in this paper, with  $o$  representing observations,  $s$  representing simulation data and  $n$  the number of observations:

- Fractional bias (range between -2 and 2, perfect value : 0):  $FB = 2\left(\frac{\bar{s}-\bar{o}}{\bar{s}+\bar{o}}\right)$
- Pearson correlation (range between -1 and 1, perfect correlation : 1):  $R = \frac{\overline{(s-\bar{s})(o-\bar{o})}}{\sqrt{(\overline{(s-\bar{s})^2})(\overline{(o-\bar{o})^2})}}$
- Spearman correlation, computed as the Pearson correlation applied to the ranks of the pairs of values compared (range between -1 and 1, perfect correlation : 1):  $r_s = \frac{\overline{(rg_s-rg_s)(rg_o-rg_o)}}{\sqrt{(\overline{(rg_s-rg_s)^2})(\overline{(rg_o-rg_o)^2})}}$
- Normalized mean square error (range higher or equal to 0, perfect value : 0):  $NMSE = \frac{\overline{(o-s)^2}}{\overline{o^2}}$

- FAC2 is the proportion of data that meets the criteria (range between 0 and 1, perfect value : 1):  $0.5 \leq \frac{s}{o} \leq 2$
- Geometric variance (range higher or equal to 1, perfect value : 1):  $VG = \exp[(\ln(o) - \ln(s))^2]$

610

### **Appendix B: Impact of the emissions and the aspect ratio of the street**

The strong correlation between the emissions and the disparities observed between MUNICH and the Subgrid method is confirmed by the Figure B1 (a) in Appendix B. The cell containing a part of the Paris ring road, leading to a wide range of emission values, presents a significantly greater range of bias values than the cell inside the city (illustrated by Figure B1 (b) in Appendix B). Indeed, we observed that for stations near the Paris ring road, namely BP\_EST, AUT, and RN2, the minimum fractional bias averages at -0.61, while the maximum reaches 1.08. In contrast, for stations within the city, the fractional bias ranges between -0.29 and 0.53 on average. This observation confirms that the discrepancies between the approaches are significantly less pronounced in areas with a more homogeneous distribution of emissions compared to those adjacent to highways, which introduce heterogeneous emissions.

615

Figures/2\_bias\_cell\_appendix.png

**Figure B1.** Bias between MUNICH and the Subgrid method for  $\text{NO}_x$ , as a function of  $\alpha_r$  (X axis) and the average emissions of MUNICH (Y axis, in  $\mu\text{g}\cdot\text{s}^{-1}\cdot\text{m}^{-2}$ ) for all the streets (points) within a cell, over February and March 2014. The left panel shows the results for the cell containing stations BP\_EST and SOULT (a), which includes part of the Paris ring road. The right panel shows the results for the cell containing HAUS (b), located within the city.



620 In order to quantify the impact of emissions on the differences observed between the two approaches studied, the Spearman's correlation defined in Appendix A is used. The Spearman's rank correlation coefficient (defined in Appendix A) between 1) the FBs in the mean concentrations (for the two months studied) calculated by the two approaches and 2) the differences,  $E_{\text{diff}}(i)$ , between the local emission in street  $i$  ( $E_i$ ) and the average of emissions over the  $N_s$  streets in the corresponding cell (weighted by street surfaces  $\{S_j\}_{j=1, N_s}$ ) is used to quantify the strength of the relationship.  $E_{\text{diff}}(i)$  is then defined as:

$$625 \quad E_{\text{diff}}(i) = E_i - \sum_{j=1, N_s} E_j \frac{S_j}{\sum_{k=1, N_s} S_k} \quad (\text{B1})$$

For  $\text{NO}_x$ ,  $\text{NO}_2$ , and  $\text{PM}_{2.5}$ , the coefficients are 0.88, 0.85, and 0.87, respectively. These values confirm a significant correlation (potentially non linear) between the emission heterogeneity and the observed disparities between the modelling approaches.

### **Appendix C: Different model evaluation criteria**

630 The tables below summarise whether each method adheres to the various criteria outlined by Herring and Huq (2018). An "O" indicates that the criteria is respected, while an "X" signifies rejection. "Sc" represents the "strict criterion", which is the most stringent, and "Lsc" corresponds to the "less strict criterion". The statistical indicator NMSE is not displayed in this appendix because not relevant in the current paper. Both approaches meet the criteria described by the Normalized Mean Squared Error (NMSE) for all the traffic stations.

Statistical indicators		NO <sub>x</sub>						NO <sub>2</sub>					
		FB		VG		FAC2		FB		VG		FAC2	
		Sc	Lsc	Sc	Lsc	Sc	Lsc	Sc	Lsc	Sc	Lsc	Sc	Lsc
BP_EST	Subgrid	X	O	X	-	X	O	O	O	O	-	O	O
	MUNICH	O	O	X	-	O	O	O	O	O	-	O	O
AUT	Subgrid	X	X	X	-	X	X	X	O	X	-	X	O
	MUNICH	O	O	O	-	O	O	O	O	O	-	O	O
RN2	Subgrid	X	O	O	-	O	O	O	O	O	-	O	O
	MUNICH	O	O	O	-	O	O	O	O	O	-	O	O
SOULT	Subgrid	X	O	X	-	O	O	X	O	O	-	O	O
	MUNICH	O	O	O	-	O	O	O	O	O	-	O	O
CELES	Subgrid	O	O	O	-	O	O	O	O	O	-	O	O
	MUNICH	O	O	X	-	O	O	O	O	O	-	O	O
ELYS	Subgrid	O	O	O	-	O	O	O	O	O	-	O	O
	MUNICH	O	O	O	-	O	O	O	O	O	-	O	O
HAUS	Subgrid	O	O	O	-	O	O	O	O	O	-	O	O
	MUNICH	O	O	O	-	O	O	O	O	O	-	O	O
BONAP	Subgrid	X	O	O	-	O	O	O	O	O	-	O	O
	MUNICH	O	O	O	-	O	O	O	O	O	-	O	O

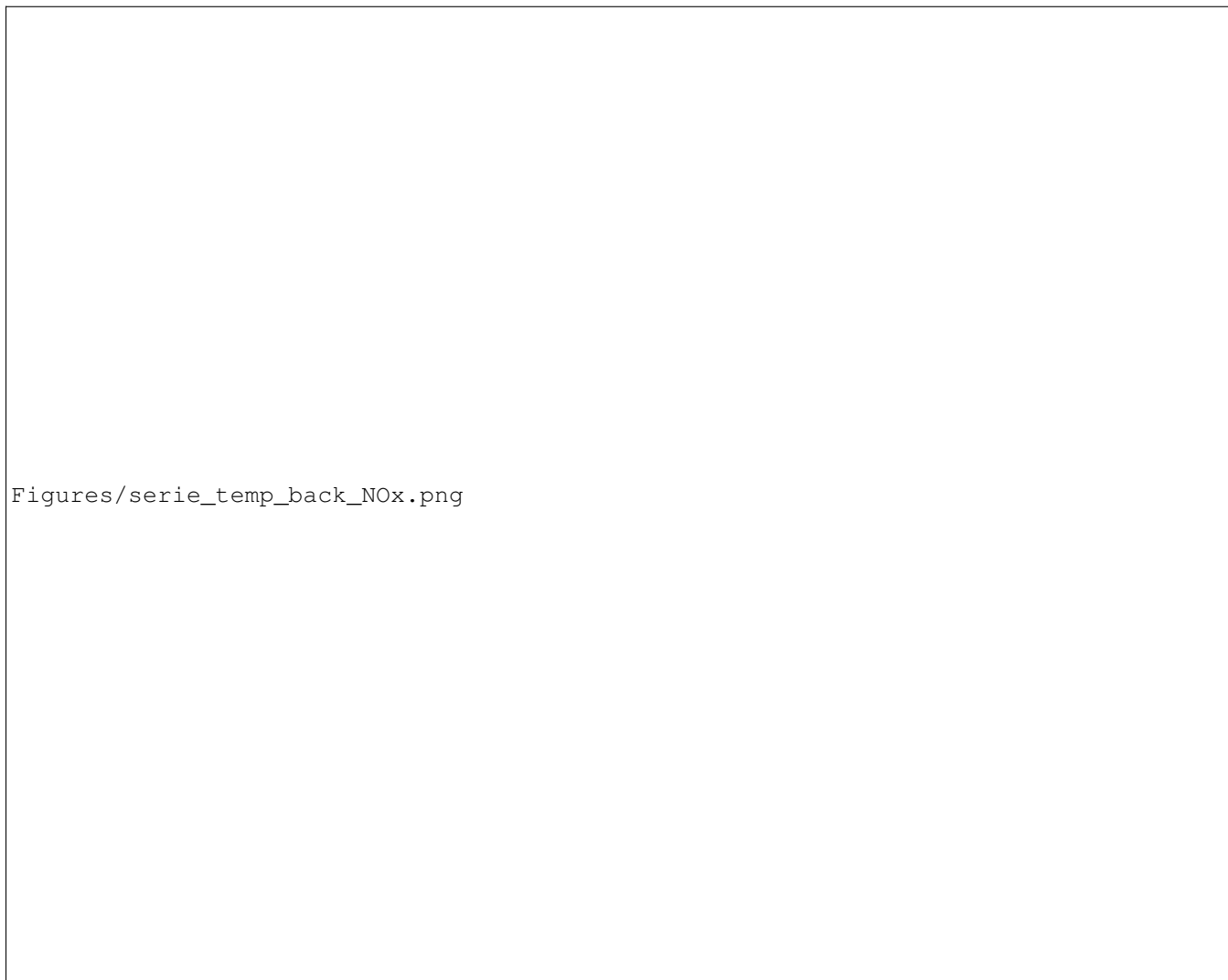
**Table C1.** Validation of the criterion from (Herring and Huq, 2018) on all the traffic stations for NO<sub>x</sub> and NO<sub>2</sub>

Statistical indicators		PM <sub>2.5</sub>					
		FB		VG		FAC2	
		Sc	Lsc	Sc	Lsc	Sc	Lsc
BP_EST	Subgrid	X	O	X	-	O	O
	MUNICH	O	O	O	-	O	O
AUT	Subgrid	X	O	X	-	O	O
	MUNICH	O	O	O	-	O	O

**Table C2.** Validation of the criterion from (Herring and Huq, 2018) on all the traffic stations for PM<sub>2.5</sub>

		NO <sub>x</sub>		NO <sub>2</sub>		PM <sub>2.5</sub>	
		NP	APE	NP	APE	NP	APE
FB	Subgrid	-0.29	-0.35	-0.02	-0.08	-0.59	-0.51
	MUNICH	-0.03	-0.03	0.06	0.1	-0.24	0.07
NMSE	Subgrid	0.79	0.87	0.29	0.27	0.67	0.78
	MUNICH	0.49	0.37	0.14	0.16	0.34	0.44

**Table C3.** Comparison of the mean of the normalized mean square error (NMSE) and the fractional bias (FB) of all the stations during a normal period (NP) and during the air pollution episode (APE), for NO<sub>x</sub>, NO<sub>2</sub> (on 8 stations) and for PM<sub>2.5</sub> concentrations (on 2 stations) simulated by the Subgrid method and MUNICH.



Figures/serie\_temp\_back\_NOx.png

**Figure D1.** Daily average concentrations observed (black dot), simulated by CHIMERE (in green) over two months, at some measurement stations, for NO<sub>x</sub> concentrations.

Figures/serie\_temp\_back\_NO2.png

**Figure D2.** Daily average concentrations observed (black dot), simulated by CHIMERE (in green) over two months, at some measurement stations, for NO<sub>2</sub> concentrations.




Figures/PM<sub>2.5</sub>\_PA04C\_\_\_ByDay.png

**Figure D3.** Daily average concentrations observed (black dot), simulated by CHIMERE (in green) over two months, at some measurement stations, for PM<sub>2.5</sub> concentrations.

## Appendix E: Evaluation of daily profiles

Figures/NOx\_\_\_\_boxplot\_day.png

**Figure E1.** Daily profiles of the bias (in  $\mu\text{g}\cdot\text{m}^{-3}$ ) between observed and simulated concentrations for the period of February-March 2014, for  $\text{NO}_x$  concentrations.



Figures/NO2\_\_\_\_boxplot\_day.png

**Figure E2.** Daily profiles of the bias (in  $\mu\text{g}\cdot\text{m}^{-3}$ ) between observed and simulated concentrations for the period of February-March 2014, for NO<sub>2</sub> concentrations.

*Author contributions.* AS wrote the draft of the manuscript with contributions from YR and MV. AS, YR and MV performed the analysis. AS and MV constructed the street-network with contribution from FD. AS conducted the CHIMERE/WRF/SSH-aerosol simulations with contributions from MV, LL, YK and KS. AS conducted the MUNICH simulations with contributions from YR, YK, KS and LL. RV provided the network emission data. AS, YR, MV, YK, KS, LL and FD reviewed the final manuscript.

640

*Competing interests.* The authors declare that they have no conflict of interest.



*Acknowledgements.* The authors would like to thank AIRPARIF for the discussions and emissions provided. We thank the TGCC (Très Grand Centre de Calcul du CEA), this work was carried out using the HPC resources of GENCI TGCC under grant no. A0130110274. Alexis Squarcioni's PhD grant is funded by the Île-de-France region as part of the "Paris Region PhD" programme.

## 645 References

- Allen, L., Lindberg, F., and Grimmond, C. S. B.: Global to city scale urban anthropogenic heat flux: model and variability, *International Journal of Climatology*, 31, 1990–2005, <https://doi.org/10.1002/joc.2210>, 2010.
- Azmi, W. N. F. W., Pillai, T. R., Latif, M. T., Koshy, S., and Shaharudin, R.: Application of land use regression model to assess outdoor air pollution exposure: A review, *Environmental Advances*, 11, 100 353, <https://doi.org/https://doi.org/10.1016/j.envadv.2023.100353>, 2023.
- 650 Beevers, S. D., Kitwiroon, N., Williams, M. L., and Carslaw, D. C.: One way coupling of CMAQ and a road source dispersion model for fine scale air pollution predictions, *Atmospheric Environment*, 59, 47–58, 2012.
- Benavides, J., Snyder, M., Guevara, M., Soret, A., García-Pando, C. P., Amato, F., Querol, X., and Jorba, O.: CALIOPE-Urban v1.0: coupling R-LINE with a mesoscale air quality modelling system for urban air quality forecasts over Barcelona city (Spain), *Geoscientific Model Development*, 12, 2811–2835, <https://doi.org/10.5194/gmd-12-2811-2019>, 2019.
- 655 Berchet, A., Zink, K., Oettl, D., Brunner, J., Emmenegger, L., and Brunner, D.: Evaluation of high-resolution GRAMM–GRAL (v15.12/v14.8) NO<sub>x</sub> simulations over the city of Zürich, Switzerland, *Geoscientific Model Development*, 10, 3441–3459, <https://doi.org/10.5194/gmd-10-3441-2017>, 2017.
- Berkowicz, R.: OSPM - A Parameterised Street Pollution Model, *Environmental Monitoring and Assessment*, 65, 323–331, <https://doi.org/10.1023/a:1006448321977>, 2000.
- 660 Briant, R., Tuccella, P., Deroubaix, A., Khvorostyanov, D., Menut, L., Mailler, S., , and Turquety, S.: Aerosol-radiation interaction modelling using online coupling between the WRF 3.7.1 meteorological model and the CHIMERE 2016 chemistry-transport model, through the OASIS3-MCT coupler, *Geosci. Model Dev.*, 10, 927–944, 2017.
- Cambridge Environmental Research Consultants: ADMS 3 User Guide, Cambridge Environmental Research Consultants, Cambridge, 2001.
- Couvidat, F., Debry, E., Sartelet, K., and Seigneur, C.: A hydrophilic/hydrophobic organic (H<sup>2</sup>O) aerosol model: Development, evaluation and sensitivity analysis, *Journal of Geophysical Research: Atmospheres*, 117, n/a–n/a, <https://doi.org/10.1029/2011jd017214>, 2012.
- 665 Couvidat, F., Bessagnet, B., Garcia-Vivanco, M., Real, E., Menut, L., and Colette, A.: Development of an inorganic and organic aerosol model (CHIMERE 2017 v1.0): seasonal and spatial evaluation over Europe, *Geoscientific Model Development*, 11, 165–194, <https://doi.org/10.5194/gmd-11-165-2018>, 2018.
- Derognat, C., Beekmann, M., Baeumle, M., Martin, D., and Schmidt, H.: Effect of biogenic volatile organic compound emissions on tropospheric chemistry during the Atmospheric Pollution Over the Paris Area (ESQUIF) campaign in the Ile-de-France region, *Journal of Geophysical Research: Atmospheres*, 108, <https://doi.org/10.1029/2001jd001421>, 2003.
- 670 Dons, E., Van Poppel, M., Kochan, B., Wets, G., and Int Panis, L.: Modeling temporal and spatial variability of traffic-related air pollution: Hourly land use regression models for black carbon, *Atmospheric Environment*, 74, 237–246, <https://doi.org/10.1016/j.atmosenv.2013.03.050>, 2013.
- 675 Dupont, J.-C., Haeffelin, M., Badosa, J., Elias, T., Favez, O., Petit, J., Meleux, F., Sciare, J., Crenn, V., and Bonne, J.: Role of the boundary layer dynamics effects on an extreme air pollution event in Paris, *Atmospheric Environment*, 141, 571–579, <https://doi.org/https://doi.org/10.1016/j.atmosenv.2016.06.061>, 2016.
- EEA: Europe’s air quality status 2023, EEA Briefing, Publications Office, <https://doi.org/10.2800/59526>, 2023.
- Fuzzi, S., Baltensperger, U., Carslaw, K., Decesari, S., van der Gon, H. D., Facchini, M. C., Fowler, D., Koren, I., Langford, B., Lohmann, U., Nemitz, E., Pandis, S., Riipinen, I., Rudich, Y., Schaap, M., Slowik, J. G., Spracklen, D. V., Vignati, E., Wild, M., Williams, M.,
- 680

- and Gilardoni, S.: Particulate matter, air quality and climate: lessons learned and future needs, *Atmospheric Chemistry and Physics*, 15, 8217–8299, 2015.
- 685 Guenther, A. B., Jiang, X., Heald, C. L., Sakulyanontvittaya, T., Duhl, T., Emmons, L. K., and Wang, X.: The Model of Emissions of Gases and Aerosols from Nature version 2.1 (MEGAN2.1): an extended and updated framework for modeling biogenic emissions, *Geoscientific Model Development*, 5, 1471–1492, <https://doi.org/10.5194/gmd-5-1471-2012>, 2012.
- Hamer, P. D., Walker, S.-E., Sousa-Santos, G., Vogt, M., Vo-Thanh, D., Lopez-Aparicio, S., Schneider, P., Ramacher, M. O. P., and Karl, M.: The urban dispersion model EPISODE v10.0 – Part 1: An Eulerian and sub-grid-scale air quality model and its application in Nordic winter conditions, *Geoscientific Model Development*, 13, 4323–4353, <https://doi.org/10.5194/gmd-13-4323-2020>, 2020.
- Hatzopoulou, M., Valois, M. F., Levy, I., Mihele, C., Lu, G., Minet, S. B. L., and Brook, J.: Robustness of Land-Use Regression Models Developed from Mobile Air Pollutant Measurements, *Environmental Science & Technology*, 51, 3938–3947, 2017.
- 690 Herring, S. and Huq, P.: A Review of Methodology for Evaluating the Performance of Atmospheric Transport and Dispersion Models and Suggested Protocol for Providing More Informative Results, *Fluids*, 3, 20, <https://doi.org/10.3390/fluids3010020>, 2018.
- Hood, C., MacKenzie, I., Stocker, J., Johnson, K., Carruthers, D., Vieno, M., and Doherty, R.: Air quality simulations for London using a coupled regional-to-local modelling system, *Atmospheric Chemistry and Physics*, 18, 11 221–11 245, [https://doi.org/10.5194/acp-18-](https://doi.org/10.5194/acp-18-11221-2018)
- 695 11221-2018, 2018.
- Hooyberghs, H., De Craemer, S., Lefebvre, W., Vranckx, S., Maiheu, B., Trimpeneers, E., Vanpoucke, C., Janssen, S., Meysman, F., and Fierens, F.: Validation and optimization of the ATMO-Street air quality model chain by means of a large-scale citizen-science dataset, *Atmospheric Environment*, 272, 118 946, <https://doi.org/10.1016/j.atmosenv.2022.118946>, 2022.
- Hourdin, F., Musat, I., Bony, S., Braconnot, P., Codron, F., Dufresne, J.-L., Fairhead, L., Filiberti, M.-A., Friedlingstein, P., Grandpeix, J.-Y., Krinner, G., LeVan, P., Li, Z.-X., and Lott, F.: The LMDZ4 general circulation model: climate performance and sensitivity to parametrized physics with emphasis on tropical convection, *Climate Dynamics*, 27, 787–813, <https://doi.org/10.1007/s00382-006-0158-0>, 2006.
- 700 Hunt, J. C. R., Leibovich, S., and Richards, K. J.: Turbulent shear flows over low hills, *Quarterly Journal of the Royal Meteorological Society*, 144, 1435 – 1470, <https://rmets.onlinelibrary.wiley.com/doi/epdf/10.1002/qj.49711448405>, 1988.
- Jiménez, P. A., Dudhia, J., González-Rouco, J. F., Navarro, J., Montávez, J. P., and García-Bustamante, E.: A Revised Scheme for the WRF Surface Layer Formulation, *Monthly Weather Review*, 140, 898–918, <https://doi.org/10.1175/mwr-d-11-00056.1>, 2012.
- 705 Karl, M., Walker, S.-E., Solberg, S., and Ramacher, M. O. P.: The Eulerian urban dispersion model EPISODE – Part 2: Extensions to the source dispersion and photochemistry for EPISODE–CityChem v1.2 and its application to the city of Hamburg, *Geoscientific Model Development*, 12, 3357–3399, <https://doi.org/10.5194/gmd-12-3357-2019>, 2019.
- Kiesewetter, G., Borken-Kleefeld, J., Schöpp, W., Heyes, C., Bertok, I., Thunis, P., Bessagnet, B., Terrenoire, E., and Amann, M.: Modelling compliance with NO<sub>2</sub> and PM<sub>10</sub> air quality limit values in the GAINS model, Tech. Rep. Thematic Strategy on Air Pollution #9, International Institute for Applied Systems Analysis, [https://previous.iiasa.ac.at/web/home/research/researchPrograms/air/policy/TSAP-Report-\\_9-v1\\_final-MA.pdf](https://previous.iiasa.ac.at/web/home/research/researchPrograms/air/policy/TSAP-Report-_9-v1_final-MA.pdf), 2013.
- 710 Kim, Y., Sartelet, K., Raut, J.-C., and Chazette, P.: Evaluation of the Weather Research and Forecast/Urban Model Over Greater Paris, *Boundary-Layer Meteorology*, 149, 105–132, <https://doi.org/10.1007/s10546-013-9838-6>, 2013.
- 715 Kim, Y., Wu, Y., Seigneur, C., and Roustan, Y.: Multi-scale modeling of urban air pollution: development and application of a Street-in-Grid model (v1.0) by coupling MUNICH (v1.0) and Polair3D (v1.8.1), *Geoscientific Model Development*, 11, 611–629, 2018.

- Kim, Y., Lugon, L., Maison, A., Sarica, T., Roustan, Y., Valari, M., Zhang, Y., André, M., and Sartelet, K.: MUNICH v2.0: a street-network model coupled with SSH-aerosol (v1.2) for multi-pollutant modelling, *Geoscientific Model Development*, 15, 7371–7396, <https://doi.org/10.5194/gmd-15-7371-2022>, 2022.
- 720 Kusaka, H., Kondo, H., Kikagawa, Y., and Kimura, F.: A Simple Single-Layer Urban Canopy Model For Atmospheric Models: Comparison With Multi-Layer And Slab Models, *Springer*, 101, 329–358, 2001.
- Lelieveld, J., Evans, J., Fnais, M., Giannadaki, D., and Pozzer, A.: The contribution of outdoor air pollution sources to premature mortality on a global scale, *Nature*, 525, 367–371, <https://doi.org/10.1038/nature15371>, 2015.
- Lenschow, P., Abraham, H.-J., Kutzner, K., Lutz, M., PreuB, J.-D., and Reichenbfigher, W.: Some ideas about the sources of PM<sub>10</sub>, *Atmospheric Environment*, 1, S23–S33, 2001.
- 725 Lian, J., Wu, L., Bréon, F.-M., Broquet, G., Vautard, R., Zaccaro, T. S., Dobler, J., and Ciais, P.: Evaluation of the WRF-UCM mesoscale model and ECMWF global operational forecasts over the Paris region in the prospect of tracer atmospheric transport modeling, *Elementa: Science of the Anthropocene*, 6, <https://doi.org/10.1525/elementa.319>, 2018.
- Lin, C., Wang, Y., Ooka, R., Flageul, C., Kim, Y., Kikumoto, H., Wang, Z., and Sartelet, K.: Modelling of street-scale pollutant dispersion by coupled simulation of chemical reaction, aerosol dynamics, and CFD, *Atmos. Chem. Phys.*, pp. 1421–1436, <https://doi.org/10.5194/acp-23-1421-2023>, 2023.
- 730 Liu, G., Sun, J., and Jiang, W.: Observational verification of urban surface roughness parameters derived from morphological models, *Meteorological Applications*, 16, 205–213, <https://doi.org/10.1002/met.109>, 2009.
- Longley, I., Somervell, E., and Gray, S.: Roadside increments in PM<sub>10</sub>, NO<sub>x</sub> and NO<sub>2</sub> concentrations observed over 2 months at a major highway in New Zealand, *Air Quality Atmosphere & Health*, 8, 591–602, 2014.
- 735 Lugon, L., Sartelet, K., Kim, Y., Vigneron, J., and Chrétien, O.: Nonstationary modeling of NO<sub>2</sub>, NO and NO<sub>x</sub> in Paris using the Street-in-Grid model: coupling local and regional scales with a two-way dynamic approach, *Atmospheric Chemistry and Physics*, 20, 7717–7740, 2020.
- Lugon, L., Sartelet, K., Kim, Y., Vigneron, J., and Chrétien, O.: Simulation of primary and secondary particles in the streets of Paris using MUNICH, *Faraday Discuss.*, 226, 432–456, <https://doi.org/10.1039/D0FD00092B>, 2021.
- 740 Lugon, L., Kim, Y., Vigneron, J., Chrétien, O., André, M., André, J.-M., Moukhtar, S., Redaelli, M., and Sartelet, K.: Effect of vehicle fleet composition and mobility on outdoor population exposure: A street resolution analysis in Paris, *Atmospheric Pollution Research*, 13, 101365, <https://doi.org/10.1016/j.apr.2022.101365>, 2022.
- Macdonald, R. W., Griffiths, R. F., and Hall, D. J.: An improved method for the estimation of surface roughness of obstacle arrays, *Atmospheric Environment*, 32, 1857–1864, 1998.
- 745 Mailler, S., Menut, L., Khvorostyanov, D., Valari, M., Couvidat, F., Siour, G., Turquety, S., Briant, R., Tuccella, P., Bessagnet, B., Colette, A., Létinois, L., Markakis, K., and Meleux, F.: CHIMERE-2017: from urban to hemispheric chemistry-transport modeling, *Geoscientific Model Development*, 10, 2397–2423, 2017.
- Maison, A., Flageul, C., Carissimo, B., Tuzet, A., and Sartelet, K.: Parametrization of Horizontal and Vertical Transfers for the Street-Network Model MUNICH Using the CFD Model Code\_Saturne, *Atmosphere*, 13, 527, <https://doi.org/10.3390/atmos13040527>, 2022.
- 750 Maison, A., Lugon, L., Park, S.-J., Baudic, A., Cantrell, C., Couvidat, F., D’Anna, B., Di Biagio, C., Gratien, A., Gros, V., Kalalian, C., Kammer, J., Michoud, V., Petit, J.-E., Shahin, M., Simon, L., Valari, M., Vigneron, J., Tuzet, A., and Sartelet, K.: Significant impact of urban-tree biogenic emissions on air quality estimated by a bottom-up inventory and chemistry-transport modeling, *EGUsphere*, accepted for publication, 1–57, <https://doi.org/10.5194/egusphere-2023-2786>, 2023.

- 755 Marcoa, A. D., Proietti, C., Anav, A., Ciancarella, L., D'Elia, I., Fares, S., Fornasier, M. F., Fusaro, L., Gualtieri, M., Manes, F., Marchetto, A., Mircea, M., Piersanti, E. P. A., Rogora, M., Salvati, L., Salvatori, E., Screpanti, A., and Leonardi, C.: Impacts of air pollution on human and ecosystem health, and implications for the national emission ceilings directive, *Insights from Italy*, *Environ. Int.*, 125, 320–333, 2019.
- Martilli, A., Clappier, A., and Rotach, M. W.: An Urban Surface Exchange Parameterisation for Mesoscale Models, *Springer*, 104, 261–304, 2002.
- 760 Menut, L., Bessagnet, B., Briant, R., Cholakian, A., Couvidat, F., Mailler, S., Pennel, R., Siour, G., Tuccella, P., Turquety, S., and Valari, M.: The CHIMERE v2020r1 online chemistry-transport model, *Geoscientific Model Development*, 14, 6781–6811, <https://doi.org/10.5194/gmd-14-6781-2021>, 2021a.
- Menut, L., Bessagnet, B., Briant, R., Cholakian, A., Couvidat, F., Mailler, S., Pennel, R., Siour, G., Tuccella, P., Turquety, S., and Valari, M.: The CHIMERE v2020r1 online chemistry-transport model, *Geoscientific Model Development*, 14, 6781–6811, 2021b.
- 765 National Centers For Environmental Prediction/National Weather Service/NOAA/U.S. Department Of Commerce: NCEP FNL Operational Model Global Tropospheric Analyses, continuing from July 1999, <https://doi.org/10.5065/D6M043C6>, 2000.
- Pantusheva, M., Mitkov, R., Hristov, P. O., and Petrova-Antonova, D.: Air pollution dispersion modelling in urban environment using CFD: A systematic Review, *Atmosphere*, 13, 1640, <https://doi.org/10.3390/atmos13101640>, 2022.
- Pigeon, G., Legain, D., Durand, P., and Masson, V.: Anthropogenic heat release in an old European agglomeration (Toulouse, France), *International Journal of Climatology*, 27, 1969–1981, <https://doi.org/10.1002/joc.1530>, 2007.
- 770 P.L.Carter, W.: A detail mechanism for the gas-phase atmospheric reactions of organic compounds, *Atmospheric Environment. Part A. General Topics*, 24, 481–518, 1990.
- Sabatino, S. D., Buccolieri, R., and Salizzoni, P.: Recent advancements in numerical modelling of flow and dispersion in urban areas: a short review, *International Journal of Environment and Pollution*, 52, 172, <https://doi.org/10.1504/ijep.2013.058454>, 2013.
- 775 Sailor, D. J., Georgescu, M., Milne, J. M., and Hart, M. A.: Development of a national anthropogenic heating database with an extrapolation for international cities, *Atmospheric Environment*, 118, 7–18, <https://doi.org/10.1016/j.atmosenv.2015.07.016>, 2015.
- Salamanca, F. and Martilli, A.: A new Building Energy Model coupled with an Urban Canopy Parameterization for urban climate simulations—part II. Validation with one dimension off-line simulations, *Springer*, 99, 2009.
- Salamanca, F., Georgescu, M., Mahalov, A., and Moustauoui, M.: Summertime Response of Temperature and Cooling Energy Demand to Urban Expansion in a Semiarid Environment, *Journal of Applied Meteorology and Climatology*, 54, 1756–1772, <https://doi.org/10.1175/jamc-d-14-0313.1>, 2015.
- 780 Salizzoni, P., Soulhac, L., and Mejean, P.: Street canyon ventilation and atmospheric turbulence, *Atmospheric Environment*, 43, 5056–5067, <https://doi.org/10.1016/j.atmosenv.2009.06.045>, 2009.
- Sarica, T., Maison, A., Roustan, Y., Ketzler, M., Jensen, S. S., Kim, Y., Chaillou, C., and Sartelet, K.: Modelling concentration heterogeneities in streets using the street-network model MUNICH, *Geoscientific Model Development Discussions*, 2023, 1–34, 2023.
- 785 Sartelet, K., Couvidat, F., Wang, Z., Flageul, C., and Kim, Y.: SSH-Aerosol v1.1: A Modular Box Model to Simulate the Evolution of Primary and Secondary Aerosols, *Atmosphere*, 11, 525, <https://doi.org/10.3390/atmos11050525>, 2020.
- Sartelet, K., Kim, Y., Couvidat, F., Merkel, M., Petäjä, T., Sciare, J., and Wiedensohler, A.: Influence of emission size distribution and nucleation on number concentrations over Greater Paris, *Atmospheric Chemistry and Physics*, 22, 8579–8596, <https://doi.org/10.5194/acp-22-8579-2022>, 2022.
- 790

- Sicard, P., Agathokleous, E., Anenberg, S. C., De Marco, A., Paoletti, E., and Calatayud, V.: Trends in urban air pollution over the last two decades: A global perspective, *Science of The Total Environment*, 858, 160064, <https://doi.org/https://doi.org/10.1016/j.scitotenv.2022.160064>, 2023.
- Skamarock, W., Klemp, J., Dudhia, J., Gill, D., Barker, D., and Wang, W.: A Description of the Advanced Research WRF Version 2, Tech. rep., UCAR/NCAR, <https://doi.org/10.5065/D6DZ069T>, 2005.
- 795 Soulhac, L., Salizzoni, P., Cierco, F.-X., and Perkins, R.: The model SIRANE for atmospheric urban pollutant dispersion part I, presentation of the model, *Atmospheric Environment*, 45, 7379–7395, <https://doi.org/10.1016/j.atmosenv.2011.07.008>, 2011.
- Stocker, J., Hood, C., Carruthers, D., and McHugh, C.: ADMS-Urban: developments in modelling dispersion from the city scale to the local scale, *International Journal of Environment and Pollution*, 50, 308, <https://doi.org/10.1504/ijep.2012.051202>, 2012.
- 800 Tewari, M., Salamanca, F., Martilli, A., Treinish, L., and Mahalov, A.: Impacts of projected urban expansion and global warming on cooling energy demand over a semiarid region, *Atmospheric Science Letters*, 18, 419–426, <https://doi.org/10.1002/asl.784>, 2017.
- Theeuwes, N. E., Ronda, R. J., Harman, I. N., Christen, A., and Grimmond, C. S. B.: Parametrizing Horizontally-Averaged Wind and Temperature Profiles in the Urban Roughness Sublayer, *Boundary-Layer Meteorology*, 173, 321–348, <https://doi.org/10.1007/s10546-019-00472-1>, 2019.
- 805 Thouron, L., Seigneur, C., Kim, Y., Legorgeu, C., Roustan, Y., and Bruge, B.: Simulation of trace metals and PAH atmospheric pollution over Greater Paris: Concentrations and deposition on urban surfaces, *Atmospheric Environment*, 167, 360–376, 2017.
- Thunis, P.: On the validity of the incremental approach to estimate the impact of cities on air quality, *Atmospheric Environment*, 173, 210–222, 2017.
- Tuccella, P., Menut, L., Briant, R., Deroubaix, A., Khvorostyanov, D., Mailler, S., Siour, G., and Turquety, S.: Implementation of Aerosol-Cloud Interaction within WRF-CHIMERE Online Coupled Model: Evaluation and Investigation of the Indirect Radiative Effect from Anthropogenic Emission Reduction on the Benelux Union, *Atmosphere*, 10, 2019.
- 810 Valari, M. and Menut, L.: Transferring the heterogeneity of surface emissions to variability in pollutant concentrations over urban areas through a chemistry-transport model, *Atmospheric Environment*, 44, 3229–3238, 2010.
- Vogel, J. and Afshari, A.: Comparison of Urban Heat Island Intensity Estimation Methods Using Urbanized WRF in Berlin, Germany, *Atmosphere*, 11, 1338, <https://doi.org/10.3390/atmos11121338>, 2020.
- 815 Wang, T., Li, J., Pan, J., Ji, D., Kim, Y., Wu, L., Wang, X., Pan, X., Sun, Y., Wang, Z., Yang, W., and Du, H.: An integrated air quality modeling system coupling regional-urban and street models in Beijing, *Urban Climate*, 43, 101 143, <https://doi.org/10.1016/j.uclim.2022.101143>, 2022.
- Wang, W.: An Analytical Model for Mean Wind Profiles in Sparse Canopies, *Boundary-Layer Meteorology*, 142, 383–399, <https://doi.org/10.1007/s10546-011-9687-0>, 2011.
- 820 Wang, W.: Analytically Modelling Mean Wind and Stress Profiles in Canopies, *Boundary-Layer Meteorology*, 151, 239–256, <https://doi.org/10.1007/s10546-013-9899-6>, 2014.
- Wang, Z., Couvidat, F., and Sartelet, K.: Response of biogenic secondary organic aerosol formation to anthropogenic NO<sub>x</sub> emission mitigation, *Sci. Tot. Environ.*, in review, 2024.
- 825 Wang, Z.-H., Bou-Zeid, E., Au, S. K., and Smith, J. A.: Analyzing the Sensitivity of WRF’s Single-Layer Urban Canopy Model to Parameter Uncertainty Using Advanced Monte Carlo Simulation, *Journal of Applied Meteorology and Climatology*, 50, 1795–1814, 2011.
- WGE: Trends in ecosystem and health responses to long-range transported atmospheric pollutants, Tech. Rep. ISBN 978-82-577-6681-8, ICP Waters, <https://unece.org/environment-policy/publications/trends-ecosystem-and-health-responses-long-range-transported>, 2016.

- 830 WHO: Review of evidence on health aspects of air pollution - REVIHAAP Project, Tech. Rep. ISBN 978-92-4-003422-8, World Health Organization Regional Office for Europe, Bonn, <https://apps.who.int/iris/handle/10665/341712>, 2013.
- WHO: WHO global air quality guidelines. Particulate matter (PM<sub>2.5</sub> and PM<sub>10</sub>), ozone, nitrogen dioxide, sulfur dioxide and carbon monoxide, Tech. Rep. ISBN 978-92-4-003422-8, World Health Organization, Geneva, <https://apps.who.int/iris/handle/10665/345329>, 2021.
- Zhang, Y., Gu, Z., and Yu, C. W.: Impact Factors on Airflow and Pollutant Dispersion in Urban Street Canyons and Comprehensive Simulations: a Review, *Current Pollution Reports*, 6, 425–439, <https://doi.org/10.1007/s40726-020-00166-0>, 2020.